THESIS

DFT CALCULATIONS FOR CADMIUM TELLURIDE (CdTe)

Submitted by

Sai Avinash Pochareddy

Department of Mechanical Engineering

In partial fulfilment of the requirements

For the Degree of Master of Science

Colorado State University

Fort Collins, Colorado

Fall 2019

Master's Committee:

Advisor: Sampath Walajabad
Co-Advisor: Chris Weinberger

James Sites

ABSTRACT

APPLYING QUANTUM ATK TO PERFORM DFT CALCULATIONS ON CADMIUM TELLURIDE (CdTe)

Cadmium Telluride (CdTe) thin film photovoltaics (PV) has demonstrated low Levelized Cost of Energy (LCOE). CdTe technology also counted for half the thin film market in 2013 [3]. CdTe PV has the smallest carbon footprint and the energy payback time (less than one year) is the shortest of any current photovoltaic technology. The modules made of CdTe can also be recycled at the end of their lifetime. The attractiveness of these materials comes from their bandgap value (1.5 eV), which falls within the solar spectrum, thereby enabling the efficient creation of electron-hole pairs (or excitons) by solar photons. This has led to the research that dates back to 1950's and is currently ongoing in many parts of the world. A simple heterojunction cell design was evolved in which p-type CdTe was matched with n-type Cadmium Sulfide (CdS) and by adding the top and bottom contacts. Today, multiple crystalline layers, of thicknesses ranging from a few nanometers (nm) to tens of micrometers (μm), are added to improve the efficiencies of the CdTe PV cells. The highest cell efficiency recorded to date is over 22%.

Different computational tools and methods are used to study these effects, with Quantum ESPRESSO and VASP being used for many years now. QuantumATK, built in 2008 by the company Atomistix and acquired by Synopsys in 2017, is a simulation tool that uses Density Functional Theory (DFT) for atomistic-scale modelling of nanostructures.

In this work, QuantumATK was used to predict the structural properties of bulk CdTe. Different exchange-correlation (XC) functionals were used to perform the calculations. Firstly, the

crystal structure of bulk CdTe was predicted using the tool. Later the properties like lattice parameter, were calculated. In addition to structural properties, the electrical properties were also predicted using different XC functionals. Also, the XC functionals that correct the bandgap obtained from the standard functionals were used to predict the bandgaps and the results were also compared to the experimental values again to see how accurately does QuantumATK predicts the electrical properties of bulk CdTe.

The LDA and GGA XC functionals, predicted the band gap for bulk CdTe with error percentages of 57% and 40 % respectively, when compared to the experimental value. The more accurate MGGA predicted the band gap with a 24% error while HSE06 (hybrid functional) predicted within 4% of experimental value. The LDA-1/2 and GGA-1/2 predicted the band gap most accurately within 2% of the compared experimental value. All the different XC functionals predicted the crystal structure correctly and the lattice parameter was within 2.2% of the experimental value.

ACKNOWLEDGEMENTS

I would like to thank Dr. Sampath Walajabad, professor in Mechanical Engineering at Colorado State University, for giving me the opportunity to work on this project. This thesis would not have been possible without the trust, support and help from my teacher and advisor. His expertise and leadership helped me to develop an understanding of this project. I would like to thank my thesis committee members, Dr. Chris Weinberger and Dr. James Sites, for their valuable time, guidance and support in this success of this project and my Master's degree.

I would like to extend my special gratitude to Dr. Umberto Martinez of Synopsys for his guidance in this project. His time and help were instrumental in completing this project. I would also like to extend my gratitude to Synopsys team for their timely webinars which helped me understand various new functionals of QuantumATK simulation tool.

I would like to extend my gratitude to Department of Mechanical Engineering for the partial funding which helped me work on this thesis. Special thanks to Anthony Nicholson, Aanad Thiyagarajan and Akash Shah, who are also working on DFT projects, for their continuous inputs, knowledge shared and constant feedback, which helped me to a great extent in completing this project. I would not have made it without their help and support.

Last but not the least, I would like to thank my parents for trusting and encouraging me in order to achieve my goals. Nothing would have been possible without the support they gave me throughout my life.

TABLE OF CONTENTS

LIST OF TABLES

LIST OF FIGURES

CHAPTER 1: INTRODUCTION

1.1 Cadmium Telluride (CdTe) photovoltaics (PV)

Thin-Film CdTe is one of the prominent photovoltaic technologies, and it is important to understand scope and impact of the CdTe photovoltaics for large scale energy generation. CdTe photovoltaics uses technology that is based on the use of a thin film layer (solar cell that is made by depositing multiple layers of photovoltaic materials, of thicknesses from a few nanometers to tens of micrometers, on a glass substrate/superstrate configuration) designed to absorb and convert sunlight into electricity. CdTe the largest field with thin films in USA. There are various installations in USA like one field in New Mexico, that generates 50 MW, other fields in California, Arizona etc. Today, we have more than 17 GW of installed CdTe around the world with most of the power being generated in USA.

Figure 1.1: CdTe PV installation in Arizona, USA (Image reproduced with permission from Dr. Sampath's CdTe lecture)

CdTe PV is the only thin film technology with lower costs than conventional solar cells made of crystalline silicon [1][2][3]. The price of electricity using CdTe have come down to below 4 ¢/kWh. Also, CdTe has arguably the lowest production cost per watt and compete to energy generations using fossil fuels. In general, thin films have inherent advantages in manufacturing, as they can be manufactured in large areas with high speeds of fabrication. Power Consumption and materials usage during fabrication is less for thin film deposition (order of 2 g/m^2). For higher band gap CdTe, the decrease in power generation at higher operating temperature is less [4]. In research, CdTe technology have achieved Cell-level efficiency over 22% and full-sized panels efficiency around 18.6 %.

Figure 1.2: CdTe PV installations around the world (Image reproduced with permission from Dr. Sampath's CdTe lecture)

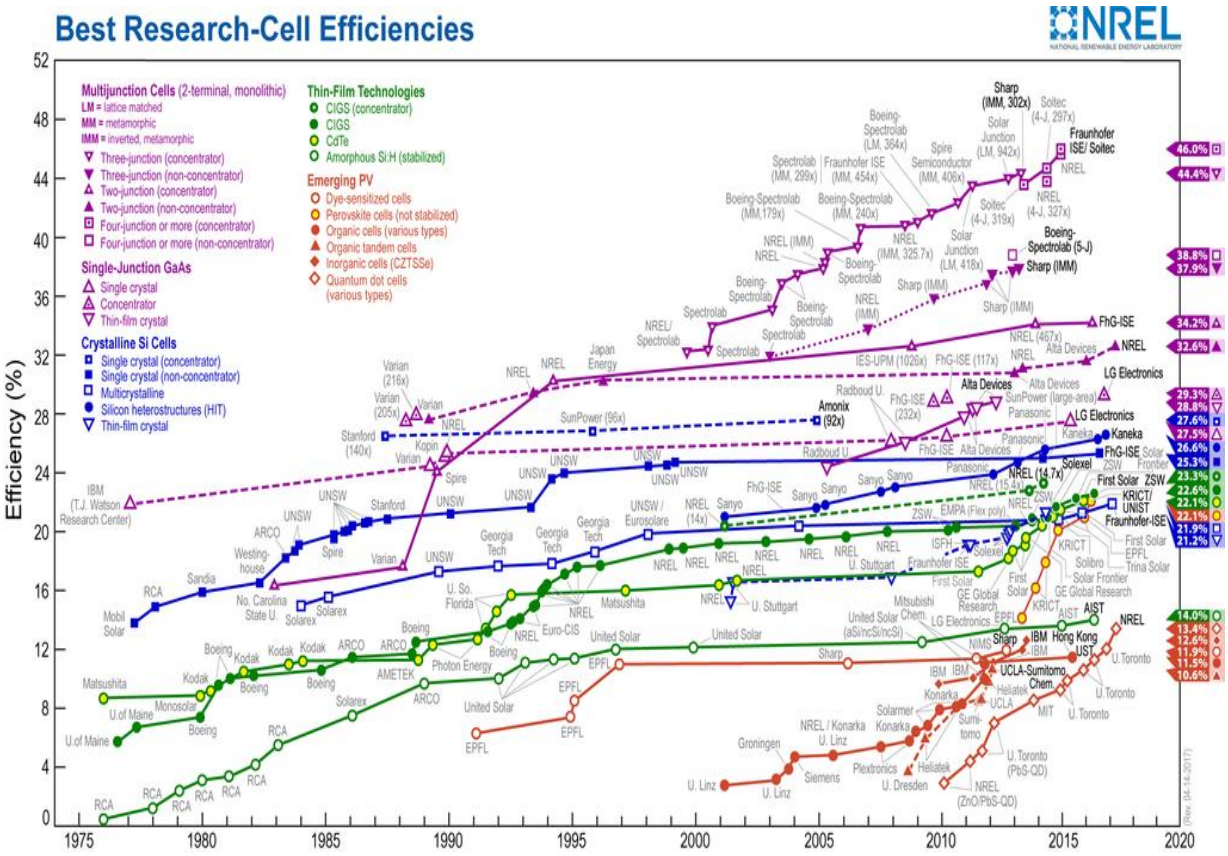

Figure 1.3: Conversion efficiencies of best solar cells worldwide for various PV technologies since 1976 (National Renewable Energy Laboratory (NREL), Golden, Co [5])

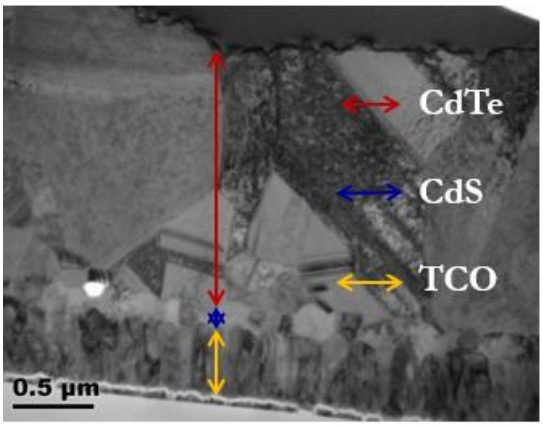

Figure 1.4: Superstrate Geometry (Image taken with permission from Dr. Sampath's Thin Film PV lecture [4])

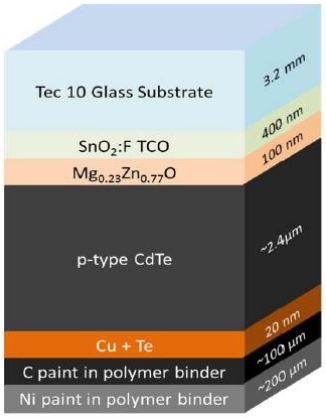

Figure 1.5: Interfaces of CdTe PV (Image reproduced with permission from Dr. Amit's CdTe lecture)

CdTe being thin film semiconductors, are polycrystalline in nature i.e. within the material there are very small crystallites about a micron and in between the crystallites are grain boundaries. Also, different PV materials are deposited on to CdTe forming a multilayer superstrate configuration. When we put all the layers together, we inherently have several interfaces. Studying the interfaces where one material must match with other is been in research focus for many years now. Computational modelling is a very useful tool in order to study these interfaces and different computational methods are being used across the globe today.

1.2 Density Functional Theory (DFT)

Density Functional Theory (DFT) is a computational method and it is effective for studying molecules, nanostructures, solids, surfaces and interfaces, by directly solving approximate versions of Schrödinger equation. We can use DFT to investigate the electronic structure (structural properties) and electronic properties of many-body systems particularly atoms, molecules and condensed phases by using electron density (spatially dependent) as a functional, hence justifying the name Density Functional Theory. DFT calculations, using ab initio methods from first principles, allow the prediction and calculation of material behavior based on quantum mechanical considerations, without requiring higher order parameters such as fundamental material properties.

1.2.1 Evolution of DFT over time

DFT was first put on firm theoretical footing by Walter Kohn and Pierre Hohenberg in the framework of the two Hohenberg-Kohn theorems in 1964 that will be discussed later in this report.

However, DFT was not considered accurate enough for calculations in quantum chemistry until 1980's, when the different approximations to calculate the Coulombic interactions were introduced and greatly refined over the years to better model the exchange and correlation interactions. One well known difficulty met by DFT calculations was the underestimating of the band gap of the materials (especially semiconductors and insulators). In 1991 Hubbard-corrected density functional theory and DFT-1/2 corrections were developed to obtain accurate band gaps in many materials including semiconductors. The algorithms, either for finding a way to separate core electrons from valence electrons, or to perform calculations for larger systems, i.e. hundreds to thousands of atoms were studied from 1966, when Phillips and Kleinman described that the electrons considered in solids is restricted to the valence electrons, which was achieved by replacing the nuclear potentials by ionic pseudopotentials. In 1979 Ionic pseudopotentials were directly incorporated within DFT, which led to first principle calculations without the core electrons, making them much faster than the earlier calculations. In 1989, algorithms to improve the studies for large systems were introduced by using linear algebra techniques in order to solve Kohn-Sham equations more efficiently. Later in early 1990's, soft pseudopotentials, projected-augmented wave and Linear-scaling DFT calculations were introduced and developed to make the computations for very large systems both cost effective and faster. Even today, relentless work and studies are going on around the world, to making DFT computations more practical and advanced [6].

1.2.2 Significance of DFT

DFT is an enabling technology for materials modelling. The DFT equations establish a most natural link between elementary quantum mechanics and materials science. The possibility of making direct and quantitative comparisons is a distinctive strength of DFT, showing that it is simple and reliable. Introducing standardized software like Quantum Espresso, VASP, Quantum ATK etc. has increased the popularity of DFT. Today, DFT software and methods are developed, used and tested by a global community. The very large size of the community is also responsible for the fast prototyping and uptake of new advances in the field. It is a wrong impression that DFT is free of shortcomings. In fact, DFT do not work for every material or every property. For instance, van der Waals binding of molecules is not described correctly, the optical absorption spectra are red-shifted, and transition metal oxides are sometimes incorrectly predicted to be metallic. Even though it fails in describing certain properties, DFT represents a reasonable starting point for more sophisticated calculations. It is often the case that, while plain DFT provides incorrect answers, some post-DFT corrections can be used in order to restore its predictive power [6][7][8][9].

1.3 Motivation

CdTe being one of the prominent photovoltaic and having a bright future it is important to understand the scope and impact of it. Over the years many researchers have been working on improving the efficiencies of the CdTe cells and eventually the full panel efficiencies. Today First solar has reached a record efficiency of 22.6% in their CdTe cells. In order to increase the efficiencies further it is important to study structural properties and electronic properties of CdTe.

Since CdTe is a multi-layer PV technology it is important to study the surfaces and interfaces of the material. With growing computational methods this is an interesting topic to focus on.

With DFT being more popular method for material modelling, the research focus would be to understand different interface properties of CdTe using DFT computations. Also, many computational tools use DFT to perform calculations. Quantum ATK is one such tool that is more popular and has high power computation skills with low costs and a friendly Graphical User Interface (GUI). Before we can use Quantum ATK for high level computing like interfaces, the interest was to see how it predicts the properties of bulk CdTe structure. This thesis presents the results of structural and electronic properties of bulk CdTe using Quantum ATK. The results of the test were analyzed, and conclusions were provided with the intent of assisting further calculations involving more complex interfacial properties while constructing an energy band alignment diagram.

1.4 Literature Review

1.4.1 Schrödinger Equation

In our introduction to DFT we stated, “DFT is effective for studying molecules, nanostructures, solids, surfaces and interfaces, by directly solving approximate versions of Schrödinger equation”. What exactly is the Schrödinger equation? According to quantum mechanics all particles in the universe are described by what is called a wavefunction and these quantum wave functions are described by Schrödinger equation. In comparison with the classical mechanics, like Force = Mass X acceleration (Newton’s second law of motion) describes the nature

of classical particles (position and momentum), the Schrödinger equation describes the nature of quantum mechanical particles. Schrödinger equation for a one particle system, can be written as,

$$-\left(\frac{\hbar^2}{2m}\right)\nabla^2\Psi + V\Psi = E\frac{\partial\Psi}{\partial t} \quad (1)$$

The term Ψ in the equation above describes the wavefunction of the quantum mechanical particles (electrons). Unlike classical particles, at a given point in time both the position and momentum of electron cannot be calculated, this is called Heisenberg's uncertainty principle. However, it is likely to calculate the probability of finding an electron ($|\Psi(r,t)|^2$) in a space at a given point in time. The probability of every possible observation is determined by the wavefunction, but prior to observation, the wavefunction changes and evolves in a completely deterministic manner [13][15][20][21]. This deterministic way in which the wavefunction behaves is what the Schrödinger equation describes. At each point in space and time, the wavefunction is a complex number with real component and an imaginary component. $\frac{\partial\Psi}{\partial x}$, indicates how much the wavefunction changes as x increases by a small amount. As we move along the x axis, the changes to the $\frac{\partial\Psi}{\partial x}$ are represented by $\frac{\partial^2\Psi}{\partial x^2}$. At each point in space, the wavefunction changes in all three dimensions and the changes along all three dimensions can be represented as sum of three complex numbers given by $\nabla^2\Psi = \frac{\partial^2\Psi}{\partial x^2} + \frac{\partial^2\Psi}{\partial y^2} + \frac{\partial^2\Psi}{\partial z^2}$ [12]. In order to understand the behavior of quantum particles, we need to determine the corresponding wavefunction Ψ (r) for every point $r = xu_x + yu_y + zu_z$ in space by solving Schrödinger equation. Here u_x, u_y, u_z indicates the unit vectors along cartesian axes.

Charged particles (electrons and nuclei) exerts forces on one another and these can be termed as coulombic interactions. These coulombic interaction between electrons and nuclei is

given by a potential energy term V in the equation (1). The kinetic energy of the particles is given by the first term in equation (1). The right-hand side of the equation corresponds to total energy. It is good starting point to restrict the discussion to stationary electronic states by which we need to consider the time-independent Schrödinger equation. So, the time-independent Schrödinger equation takes the form:

$$(Kinetic\ Energy + Potential\ Energy)\Psi(r) = E\Psi(r) \tag{2}$$

E, is the energy eigenvalue for the stationary state described by the wavefunction Ψ. The probability of finding the electron at the point r is $|\Psi(r)|^2$. When we discuss many electrons and many nuclei, we need to define a many body wavefunction, which depends on positions of each electron and each nucleus in the system. For N electrons and M nuclei,

$$\Psi = \Psi(r_1, r_2, \ldots., r_N; R_1, R_2, \ldots. R_M) \tag{3}$$

$|\Psi(r_1, r_2, \ldots., r_N; R_1, R_2, \ldots. R_M)|^2$ represents the probability of simultaneously finding electron number 1 at point r_1, electron number 2 at r_2 and so forth. The probability of finding any electron at position r, can be represented by electron density $n(r)$. It can be represented as [6],

$$n(r) = 2\Sigma_i \Psi_i^*(r)\Psi_i(r) \tag{4}$$

Here, the summation goes over all the individual electron wavefunctions that are occupied by the electrons (1to N). The term inside the summation is the probability that an electron in individual wavefunction $\Psi_i(r)$ is located at position r. The factor of 2 appears because electrons have spin and the Pauli Exclusion Principle states that each individual electron wavefunction can be occupied by two separate electrons provided they have different spins [14][18][19][20].

We have seen from equation (2) the Schrödinger equation represents the total energy of the many body system as sum of kinetic energies of electrons and nuclei and Coulombic potential energies that are determined from Coulombic repulsions between pairs of electrons and pairs of nuclei and also from the Coulombic attractions between electrons and nuclei. We use Hartree atomic units to represent the Schrödinger equation in a simple way. Therefore, the many body Schrödinger equation can be written as:

$$\left[-\Sigma_i\left(\frac{\nabla_i^2}{2}\right)-\Sigma_I\left(\frac{\nabla_I^2}{2M_I}\right)+\frac{1}{2}\Sigma_{i\neq j}\frac{1}{|r_i-r_j|}+\frac{1}{2}\Sigma_{I\neq J}\frac{Z_I Z_J}{|R_I-R_J|}-\Sigma_{i,I}\frac{Z_I}{|r_i-R_I|}\right]\Psi=E_{total}\,\Psi \qquad (5)$$

1.4.2 Approximations to Schrödinger Equation

When we solve the equation (5) to find the eigenstate with the lowest energy, which is called the ground state of the system, with which we can calculate many equilibrium properties of materials. However, the difficulty lies in solving such a complex equation. In the simplest systems (with a few electrons) to find the solution to equation (5) is very challenging, and in most cases, it is still practically impossible. One possible way to solve the equation would be to discretize the space into the uniform mesh of points by which we can transform the problem into a linear system by using finite differences for the derivatives. Let us take an example of the unit cell of Carbon (C) crystal. The volume of unit cell of carbon in diamond structure is $(a^3/4)$ with a=3.57 Å. If the unit cell is discretized such that the points are spaced by $\Delta x = 0.1$ Å, then such a grid would have consisted of $N_p = (a^3/4)/(\Delta x^3)$ which is ≈ 11,500 points. Considering a diatomic carbon molecule, each carbon atom has four valence electrons, and two nuclei, i.e. N + M= 8+2=10, the complete specification of a quantum state requires $\left(N_p\right)^{N+M} \approx 4x10^{40}$ complex numbers.

Performing matrix operations of this size is not possible. The complexity of equation (5) increases exponentially with the size of the system.

In order to solve this complex equation certain approximations are made to simplify the equation. If observed carefully we can see that most of the troubles in the study of materials from first principles arise the Coulomb repulsions between electrons. Hence, following assumptions are made to the many body Schrödinger equation [6].

1.4.2.1 Clamped Nuclei Approximation

It is used to separate the quantum mechanical motion of the electrons from the motion of the nuclei, using the fact that mass of nuclei is of higher orders compared to that of electrons. This approximation is also called as Born-Oppenheimer approximation. While in study of liquids and gases the nuclei can travel long distances, when we study solids surfaces, the nuclei typically remain very close to each other. Therefore, as a starting point, we can assume that the nuclei are held immobile i.e. they are clamped [29]. Since, the mass of nuclei is too heavy, and they are clamped we can set $M_I = \infty$ in equation (5) and the Coulomb repulsion between the nuclei is constant. We can now define:

$$E = E_{total} - \frac{1}{2}\Sigma_{I \neq J} \frac{Z_I Z_J}{|R_I - R_J|} \tag{6}$$

Also, we can consider the nuclear coordinates, R_I, as external parameters and Ψ as a function of the electron coordinates [30][31][32]. Therefore, $\Psi = \Psi(r_1, r_2, \ldots, r_N)$. The Coulomb potential of the nuclei experienced by the electrons:

$$V_n(r) = -\Sigma_I \frac{Z_I}{|r - R_I|} \tag{7}$$

From equation (6) and (7) we can rewrite the equation as:

$$\left[-\Sigma_i\left(\frac{\nabla_i^2}{2}\right)+\Sigma_i V_n(r_i)+\frac{1}{2}\Sigma_{i\neq j}\frac{1}{|r_i-r_j|}\right]\Psi = E\,\Psi \tag{8}$$

This is the fundamental equation of electron structure theory [6].

The left-hand side of the equation (8) can be represented as:

$$\hat{H}\,(r_1, r_2 \ldots, r_N) = -\Sigma_i\left(\frac{\nabla_i^2}{2}\right)+\Sigma_i V_n(r_i)+\frac{1}{2}\Sigma_{i\neq j}\frac{1}{|r_i-r_j|} \tag{9}$$

Where $\hat{H}$ is called the many electron Hamiltonian. So, the many body Schrödinger equation can simply be written as:

$$\hat{H}\Psi = E\Psi \tag{10}$$

1.4.2.2 Independent Electron Approximation

In this approximation we do not consider electron-electron interaction in a crystal i.e. the Coulomb repulsions are not included. Since, this is the only possible form of interactions between electrons, if it were absent then the electron would not see each other. So, we can say the electrons are independent. We use this approach because, firstly, we are not aware of the wavefunctions of every electron, secondly, the potential due to electron-electron interactions is not periodic and finally, we need to consider the dynamics of all the electrons at once which is a complex process [24][27]. Hence, it is natural to define single electron Hamiltonian:

$$\hat{H}_0(r) = -\frac{1}{2}\nabla^2 + V_n(r) \tag{11}$$

And the Schrödinger equation within the independent electron approximation becomes:

$$\Sigma_i \hat{H}_0(r_i)\Psi = E\Psi \tag{12}$$

The wave function can be written as:

$$\Psi(r_1, r_2, \ldots . r_N) = \phi_1(r_1)\phi_2(r_2) \ldots . \phi_N(r_N) \tag{13}$$

Where, $\phi_i(r_i)$ is the wavefunction of individual electrons. The probability of finding the many electrons simultaneously is given by $|\Psi(r_1, r_2, \ldots ., r_N)|^2$, it can be determined by the product of the individual probabilities $|\phi_i(r_i)|^2$. If the wavefunctions, ϕ_i, were considered the solutions for the single-electron Schrödinger equations, then

$$\Sigma_i \hat{H}_0(r_i)\phi(r_i) = \Sigma\varepsilon_i\phi(r_i) \tag{14}$$

With ε_1 the smallest eigenvalue and $\varepsilon_1 < \varepsilon_2 < \cdots \varepsilon_N$. Since, the single electron Hamiltonian in equation (14) acts one individual wavefunction, the resulting energy can be written as:

$$E = \varepsilon_1 + \varepsilon_2 + \cdots \varepsilon_N \tag{15}$$

This implies that, in the independent electron approximation, the lowest electron configuration of the system is obtained when we fill the lowest-energy eigenstates of the single-particle equation with one electron in each state, starting from the lowest eigenvalue.

However, the independent electron approximation carries a drawback. That is the Coulomb term eliminated is actually of the same magnitude as the other terms, and therefore it cannot be ignored. So, we make the following approximations to bring back the interactions between the electrons.

1.4.2.3 Mean-Field Approximation

Ignoring the Coulomb repulsions between the electrons is drastic and at the same time convenient for practical calculations. It will be useful if we can maintain the single particle description and take the Coulomb repulsions into consideration.

We know, in classical electrostatics, the distribution of electronic charge $n(r)$, will generate an electrostatic potential $\varphi(r)$ through Poisson's equation.

$$\nabla^2 \varphi(r) = 4\pi\, n(r) \tag{16}$$

The electrons immersed in electrostatic potential have a potential energy $V_H(r) = -\varphi(r)$ (since we are using Hartree atomic units). This potential energy is called Hartree potential and it satisfies Poisson's equation.

$$\nabla^2 V_H(r) = -4\pi\, n(r) \tag{17}$$

Taking Pauli's exclusion principle, when the electrons have different spin, we use the wavefunctions such that they have opposite signs. We can build a Slater determinant from which we can calculate the charge density of electrons as:

$$n(r) = \Sigma_i |\phi_i(r)|^2 \tag{18}$$

Since, every electron in the system experiences the Hartree potential, we can write:

$$\left[-\frac{\nabla^2}{2} + V_n(r) + V_H(r)\right]\phi_i(r) = \varepsilon_i \phi_i(r) \tag{19}$$

V_H is the average potential experienced by each electron, and hence this approach is called mean-field approximation and the idea of this theory is to replace all interactions of all electrons

with an average field. The equations (17), (18), (19) should be solved simultaneously using iterations.

The approximations used so far will simplify our initial task of solving many body Schrodinger equation, since one differential equation in 3N dimensions has been replaced by N three-dimensional equations. This reduces the number of ways of describing the wavefunctions significantly. However, the mean-field approximation would be great if the electrons were classical particles and this approximation is not accurate for quantitative study of materials at atomic scale. In order to be quantitative we need to consider the exchange and correlation potentials of electronic interactions.

1.4.3 Hartree-Fock Equations

The Hartree-Fock equations are determined by assuming that, the interactions of electrons can be solved using a Slater determinant (derived using Pauli's exclusion principle). The lowest energy E, of the quantum state ψ can be obtained by:

$$E = \int dr_1 dr_2 \dots dr_N \, \psi^* \hat{H} \psi \tag{20}$$

We can represent equation (20) using Dirac notation, $E = \langle \psi | \hat{H} | \psi \rangle$.

If we minimize the energy E with respect to variations of functions $\phi_i(r)$ in the Slater determinant and requires that these functions are orthonormal. Then we obtain the Hartree-Fock equations from the functions [36][40].

$$\int dr \;\; \phi_i^*(r) \, \phi_j(r) = \delta_{ij} \tag{21}$$

Where $\delta_{ij}$is the Kronecker delta which is equal to 1 when $i = j$ and equal to 0 when $i \neq j$.

$$\left[-\frac{\nabla^2}{2} + V_n(r) + V_H(r)\right]\phi_i(r) + \int dr' V_X(r.r')\phi_i(r') = \varepsilon_i\phi_i(r) \qquad (22)$$

$$V_X(r,r') = -\Sigma_j\left(\frac{\phi_j^*(r')\phi_j(r)}{|r-r'|}\right) \qquad (23)$$

The sum runs over the occupied single particle states. By using Hartree-Fock equations we moved from classical electrons in the mean-field approximation to quantum electrons. V_X is the non-local potential because its evaluation involves the integration over the additional variable r' and complicates the solution for Hartree-Fock equations. Potential V_X arises precisely from Pauli's exclusion principle and prevents two electrons from occupying the same quantum state and is called Fock exchange potential. It introduces the exchange interactions of the electrons into the independent electron approximated Schrödinger equation [37][38].

The only remaining element to be considered is the correlation between electrons. Correlation describes how the probability of finding an electron at a point r is affected in the presence of another electron close to that point r. We will introduce the correlation term when we discuss about Kohn-Sham equations later in this report.

1.4.4 Hohenberg and Kohn Theorems

Hohenberg-Kohn theorems relate to any system consisting of electrons moving under the influence of the external potential $V_{ext}(r)$. The many body Schrödinger equation determined from various approximations in previous sections have electrons moving under the influence of nuclei that are clamped. The structure of Hamiltonian in equation (20) is independent of material under

consideration, therefore any change in E must be associated with changes in the many body wavefunctions Ψ. We can say that Energy is functional of Ψ i.e. $E = \mathrm{F}(\Psi)$, when E is the energy of excited states [41].

First Hohenberg-Kohn theorem, states that "If E is the lowest possible energy of the system i.e. the energy of the ground state, then E is a unique functional of Electron density":

$$E = F[n(r)] \tag{24}$$

The consequence of the above statement is that in order to calculate the total energy E in the ground state, electron density is the only required quantity. The proof of the statement is based on three premises,

1.) The external potential of the nuclei V_n is uniquely determined by the electron density in the ground state.
2.) This external potential determines uniquely the many electron wavefunction Ψ, in any quantum state.
3.) In any quantum state the total energy E, is a functional of many body wavefunction Ψ.

By combining three premises we can say that, in ground state, the density uniquely determines the total energy: n→ V_n→ Ψ → E. The third premise simply reinstate equation (20) and the second premise means that if we change the positions of nuclei, we will obtain different many body wavefunction. In order to prove first premise, we assume that the same ground state electron density can be obtained from two different external potentials. If we can show our assumption leads to contradiction, then we can say the first premise is valid. To do that the kinetic energy and potential energy terms are introduced.

$$\hat{T} = -\Sigma_i \frac{1}{2} \nabla_i^2, \quad \hat{W} = \frac{1}{2} \Sigma_{i \neq j} \left(\frac{1}{|r_i - r_j|} \right) \tag{25}$$

Using this we can write the total energy notation as follows:

$$E = \int dr\, n(r) V_n(r) + \langle \psi | \hat{T} + \hat{W} | \psi \rangle \tag{26}$$

Now, let us assume that Ψ is the ground state wavefunction for the potential V_n, with Energy E and density n [36]. If there exist another external potential $V_n' \neq V_n$, which generates the same density n. $\hat{H}', \Psi' \& E'$ are the Hamiltonian, ground state wavefunction and the ground state energy corresponding to the new potential. Since, Ψ is not the ground state of the V_n' we can write:

$$E' < \int dr\, n(r) V_n'(r) + \langle \psi | \hat{T} + \hat{W} | \psi \rangle \tag{27}$$

Combining equations (26) and (27):

$$E - E' > \int dr\, n(r) [V_n(r) - V_n'(r)] \text{ or}$$

$$E' - E > \int dr\, n(r) [V_n'(r) - V_n(r)]$$

Since we did not make any assumptions for external potentials. As a result, adding up the last two equations obtain, 0>0. This is a contradiction and our assumption that the two different potentials give same ground state density is false. This proves that the first premise stated above is valid for the ground state energy.

The second Hohenberg-Kohn theorem states that "The ground state energy can be obtained variationally: the density that minimizes the total energy is the exact ground state density". This property is called Hohenberg-Kohn variational principle [39]. Although, these Hohenberg-Kohn theorems do not offer a way of computing the ground state density of a system, they play crucial

role in formulating Kohn-Sham equations that are useful for deriving simple method for carrying DFT calculations.

1.4.5 Kohn-Sham Equations

In 1965 Kohn and Sham took the total energy in the independent electron approximation as the combination of kinetic and Coulomb energy of independent electrons and the exchange and correlation energy that accounts for all the difference. The kinetic energy term in the Kohn-Sham equation is non-interacting kinetic energy because if density is written as the product of orbital densities then the kinetic energy will be the sum of all the one electron kinetic energies associated with those orbitals. The Coulomb energy of electrons can be written as sum of the external potential acting on each electron (potential by nuclei), the Hartree energy due to the presence of the average field created by all electrons acting on one electron and the term that accounts for all the exchange and correlation energy between the electrons. Hence, the Kohn-Sham equation can be represented as:

$$E = F[n] = \int drn(r)V_n(r) - \Sigma_i \int dr\phi_i^*(r)\ \frac{\nabla^2}{2}\phi_i(r) + \frac{1}{2}\iint dr\ dr'\left(\frac{n(r)n(r')}{|r-r'|}\right) + E_{xc}[n] \qquad (28)$$

It simply means that all the unknown parts of electron-electron interactions are consider under on term called exchange and correlational. The exchange and correlational energies are needed to be calculated to find the total energy of the system in the ground state, $E = F[n]$. Since all the terms in equation (28) depends on electron density, therefore it is required to calculate the electron density in order to solve the equation.

According to Hohenberg-Kohn variational principle, the ground state electron density, n_0, is precisely the function that minimizes the total energy, $E = F[n]$ and can be expressed as:

$$\frac{\delta F[n]}{\delta n}\Big|_{n_0} = 0 \tag{29}$$

This is analogous to the variational principle that is used to write Hartree-Fock equations.

The functional derivative which is equal to zero leads to an equation for the wavefunctions, $\phi_i(r)$ (from Hartree-Fock equations). These wavefunctions can be used to construct the density. Since, we require these wavefunctions to be orthonormal. Using this, the Hohenberg-Kohn variational principle leads to:

$$\left[-\frac{1}{2}\nabla^2 + V_n(r) + V_H(r) + V_{xc}(r)\right]\phi_i(r) = \varepsilon_i\phi_i(r) \tag{30}$$

The term V_{xc} is given by:

$$V_{xc}(r) = \frac{\delta E_{xc}[n]}{\delta n}\Big|_{n(r)} \tag{31}$$

$V_{xc}(r)$ is called the Exchange and correlational potential. The set of equations given in equation (30) are called Kohn-Sham equations. These equations are very powerful in calculating many properties of materials.

1.4.6 Exchange and Correlation Functionals

The Kohn-Sham method is an established quantum theory based on electron density and an exchange -correlation functional. It is therefore difficult to assess the reliability of the Kohn-Sham method without considering the appropriate exchange-correlation functional. The practical

usefulness of ground state DFT depends entirely on whether approximations for the functional $E_{xc}[n]$ could be found, which are sufficiently simple and accurate. Since, the introduction of Kohn-Sham a great lot work has been put into constructing accurate exchange-correlation functionals. $E_{xc}[n]$ in order to solve the Kohn-Sham equation. The $E_{xc}[n]$ is the only part that is approximated in the Kohn-Sham equation. A variety of exchange-correlation functionals are thus far been developed based on different physical models, out of which the more popular ones are discussed in this report.

1.4.6.1 Local Density Approximation (LDA)

LDA is the simplest approximation that is a functional of local density $n(r)$. The general form for exchange and correlation energy using LDA is given as [33]:

$$E_{xc}^{LDA}[n] = \int n(r)\, \varepsilon_{xc}^{LDA}\big(n(r)\big)dr \tag{32}$$

We can study the homogeneous electron gas system in order to construct LDA. For the homogenous electron gas the exact exchange energy can be calculated. However, the correlation term is determined by numerical terms. We can apply the exchange energy and correlation energy of homogenous electron gas model to the real system by considering the regions where the density is slowly varying (in the real system).

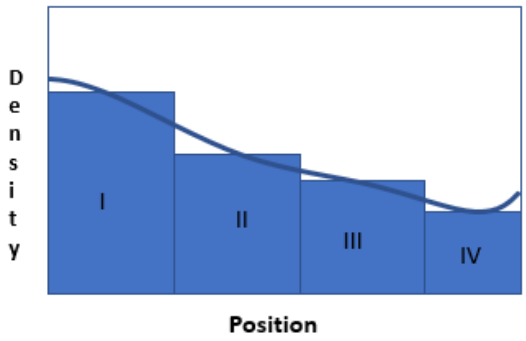

Figure 1.6: Electron density n(r) in a real system in a given direction (Image reproduced from reference [6])

Each volume element (I, II, III and so on) can be assumed as a homogenous electron gas system with local density $n(r)$ at point r. The sum of exchange energies of each small volume homogenous electron gas gives the exchange energy of that small volume elements. The exchange and correlation energy of entire system is obtained by adding all the infinitesimal volume elements. The exchange term is given by:

$$E_x^{LDA} = -\frac{3}{4}\left(\frac{3}{\pi}\right)^{\frac{1}{3}} \int_V n^{\frac{4}{3}}(r)dr \tag{33}$$

In contrast there is no simple analytical expression for correlation energy between electrons for neither an electron gas model nor for a real system. Various numerical expressions for correlation energy for real systems were constructed over years and the most common among those is Perdew and Wang (PW) (Perdew and Wang et al. 1992), which uses Wigner-Seitz radius for convenience.

$$E_c^{PW-LDA_{[n]}} = -2a\int d^3rn(1-\alpha r_s)\ln\left[1+\frac{1}{2a\left(\beta_1 r_s^{\frac{1}{3}}+\beta_2 r_s+\beta_3 r_s^{\frac{3}{2}}+\beta_4 r_s^2\right)}\right] \quad (34)$$

Where, a = 0. 031097, α = 0. 21370, β_1 = 7. 5957, β_2 = 3. 5876, β_3 = 1. 6382, and β_4 = 0. 49294 [49][51][52].

1.4.6.2 Generalized Gradient Approximation (GGA)

GGA functional are a class of semi-local approximations for the exchange-correlation energy, where the functional depends on both the local electron density value and the local gradient of it. The general expression for GGA is:

$$E^{GGA}[n] = \int n(r)\,\varepsilon^{GGA}\big(n(r),\nabla\, n(r)\big)dr \quad (35)$$

GGA exchange functionals are characterized by their differences in the region of low electron density and/or high-density gradient. This difference is attributed to the lack of fundamental physical conditions for exchange energy in the low density/high density gradient region, in contrast to the exact local density and the generalized gradient approximation limits of exchange energy, which control the high density/low density gradient regions. Since this indicates that the exchange energy in the low density/high density gradient region is restricted by no fundamental physical condition, the exchange functional forms in these regions have been determined to improve the reproducibility's of properties [50]. The common GGA exchange energy term and correlation energy term are given by Perdew (PBE) in 1996:

$$E_x = -\frac{1}{2}\Sigma_\sigma \int n(r)^{\frac{4}{3}} K_\sigma d^3r \quad (36)$$

Where $K_\sigma$is a dimensionless coefficient and is expressed using x_σ, which is a dimensionless parameter. x_σ, is defined as [50],

$$x_\sigma = \frac{|\nabla n_\sigma|}{n_\sigma^{\frac{4}{3}}} \quad (37)$$

The Correlation Energy term [50];

$$E_c^{PBE}[n, \zeta, t] = E_c^{PW-LDA_{[n]}} + \int d^3r \, nH[n, \zeta, t] \quad (38)$$

Where,

$$\zeta = \frac{n_\alpha - n_\beta}{n_\alpha + n_\beta} \quad (39)$$

1.4.6.3 Meta-GGA (MGGA)

The MGGA functional improves the GGA approximation by additionally depending on one or both, Laplacian of the density and the kinetic energy density.

Laplacian density term, $\nabla^2 n(r)$ and kinetic energy term, $\frac{1}{2}\Sigma_\alpha f_\alpha |\nabla \psi_\alpha(r)|^2$.

The term, meta-GGA functional first appeared in the PKZB meta-GGA exchange-correlation functional (Perdew et al.1999). The PKZB exchange functional intends to enhance the PBE-GGA functional using the kinetic energy density based on the fundamental conditions extended to the density Laplacian. The PKZB correlation functional removes the self-interaction error of the PBE-GGA correlational functional to reproduce the one-electron self-correlation energy. This makes it possible not only to produce more accurate exchange-correlation energies but also to estimate the contribution of the kinetic energy terms. The SCAN functional used in

the calculations has the above properties and is more computationally feasible. There are other meta-GGA exchange correlation functionals which take higher calculation times due to the semi-empirical parameters used in those functionals [50].

1.4.6.4 Hybrid Functionals

Hybrid functionals mix the Hartree–Fock exchange integral with GGA exchange functionals at a constant ratio, which makes the Kohn–Sham energies of the independent electron model link to those of the fully interacting electron one. That is, hybrid functionals are constructed by connecting exchange functionals, which are assumed as the exchange energies of the independent electron systems, to the Hartree–Fock exchange integral, which are taken as the exchange energies for the fully interacting systems.

The HSE hybrid functional extends the PBE exchange correlational functional by mixing the Hartree-Fock exchange integral only for the short-range part. The Lack of long-range exchange interactions is one of the major problems of GGA exchange functionals. However, the long-range correction for GGA exchange functionals yields much larger high occupied molecular orbitals (lower energy)–lower unoccupied molecular orbitals (higher energy) gaps for semiconductors than the corresponding experimental band gaps. Since, in HSE functional, only short range part of Hartree-Fock exchange integral is mixed in the GGA exchange functionals high occupied molecular orbitals–lower unoccupied molecular orbitals gaps calculated approaches the experimental band gaps in semiconductors and should be calculated intrinsically in excited state calculations such as time dependent Kohn-Sham calculations. HSE functional is represented as:

$$E_{xc}^{HSE} = aE_x^{SR-HF} + (1-a)E_x^{PBE} + E_c^{PBE} \quad (40)$$

Where E_x^{SR-HF} is the short-range part of the Hartree-Fock exchange integral and $a = \frac{1}{4}$ [50]. The hybrid functionals are computationally demanding, which prohibits their application to large system of atoms.

1.4.6.5 DFT-1/2 Correction to Exchange and Correlation Functionals

In extended systems, DFT-1/2, a semi-empirical approach, is used to correct the self-interacting error in local and semi-local exchange correlation density functionals. DFT-1/2 is often denoted as LDA-1/2 and GGA-1/2. This approach helps in improvement of the description of conduction band energy levels and band gaps. However, this method is not suitable for the calculations such as geometry optimization, that rely on the total energy and forces.

Slater half-occupation technique which describes a self-consistent calculation with half an electron removed from the system and taking the eigen value of the half-filled state as an estimate for the ionization energy. Its formalization was made through Janak's theorem [38] which is,

$$\frac{\partial E}{\partial f_\alpha} = e_\alpha(f_\alpha) \quad (41)$$

Where E is the total energy of the system and f_α is a function of the occupation of the one-particle Kohn and Sham state α. The Janak theorem refers to the derivative of the total energy with respect to the occupation, which equals the Kohn-Sham eigenvalue. DFT-1/2 method makes use of the theoretical insights from the half-occupation scheme and Janak's theorem to tackle the fundamental problem of the self-interaction energy. The derivation of LDA-1/2 functional using Slater half-occupation technique is elaborately explained in reference [51]. The results show that

LDA-1/2, using Self-Interaction Correction (SIC), corrects the DFT self-interacting error by defining an atomic self-energy potential that cancels the electron-hole self-interaction energy. This potential is calculated for local atomic sites in the system and is defined as the difference between the potential of the neutral atom and that of a charged ion resulting from the removal of a fraction of its charge, between 0 and 1 electrons. The total self-energy potential is the sum of these atomic potentials [23]. The addition of the DFT-1/2 self-energy potential to the DFT Hamiltonian has been found to greatly improve band gaps for a wide range of semiconductors. The half-ion technique is described in detail in [54], was used to calculate the total energies using both the LDA and GGA exchange correlation functionals. However, the fractional charge f_α removed from the neutral atom and the radius (cutoff radius r^{cut}) beyond which the atomic self-energy potential is trimmed must be fixed. r^{cut} can be fixed variationally, by selecting the value which maximizes the band gap. f_α is treated as empirical parameter and is varied by comparison with experiment. The results show that LDA-1/2 and GGA-1/2 functionals increases the band gaps in semiconductors compared to the LDA and GGA (local and semi-local) exchange correlation functionals which underestimate the band gaps heavily. Also, these functionals leads to computational efforts that are not more than standard LDA or GGA.

1.4.7 Self-Consistence Field (SCF)

The practical usefulness of ground-state DFT depends entirely on using the exchange correlation energy functionals, that includes all many body principle effects, which are at the same time sufficiently simple and accurate. Considering a right exchange correlation energy functional is used, we can calculate the exact exchange correlation potential. The next step would be solving

the single particle Schrödinger equation defined by Kohn-Sham equations. The Kohn-Sham equations (from equation (30)) are rewritten below [6].

$$\left[-\frac{1}{2}\nabla^2 + V_{total}(r)\right]\phi_i(r) = \varepsilon_i\phi_i(r)$$

$$V_{total}(r) = V_n(r) + V_H(r) + V_{xc}(r) \tag{42}$$

The standard single point Schrödinger equation can be solved as standard eigenvalue problem. In order to determine the eigenfunctions, $\phi_i(r)$, and the eigenvalues ε_i. We need to know the total potential in equation (42). The $V_H(r), V_{xc}(r)$, depend on the density, n. The density is again dependent on unknown eigenfunctions $\phi_i(r)$, i.e. each solution ϕ_i is depends implicitly on all other solutions ϕ_j, describing the occupied electronic states. This means that all the solution must be determines in a self-consistent method. Self-consistency means that, if we insert the solutions ϕ_i, in electron density equation, the calculated density is used to determine the corresponding total potential in equation (42) and solve the Schrödinger equation, then we find the same function ϕ_i from which we started.

To solve the Kohn-Sham equations, we first specify the nuclear coordinates in order to obtain the nuclear potential $V_n(r)$. Now an assumed value for electron density is used to determine approximate Hartree and exchange and correlation potentials, $V_H(r)$ & $V_{xc}(r)$ respectively. The simple and useful guess for the electron density will be to add the densities of completely isolated atoms, corresponding to the position of them in the material under consideration. With the $V_n(r), V_H(r)$ & $V_{xc}(r)$ calculated, we can determine the numerical solution of the Kohn-Sham equations. This can be done for example discretizing the space into a mesh of points and representing a Laplace operator using finite difference formulas. By solving the Koh-Sham, equations we obtain the new wavefunctions ϕ_i, which can be used to construct a better estimate of

density and the total potential. These iterations continue till the new density matches the old density within an acceptable tolerance. Once, we calculate the electron density in ground state, $n(r)$, it is possible to calculate the total energy E of the system, as it is functional of ground state electron density (equation (28)). This self-consistent method is illustrated in figure 7. Hence DFT is called Self Consistent Field (SCF).

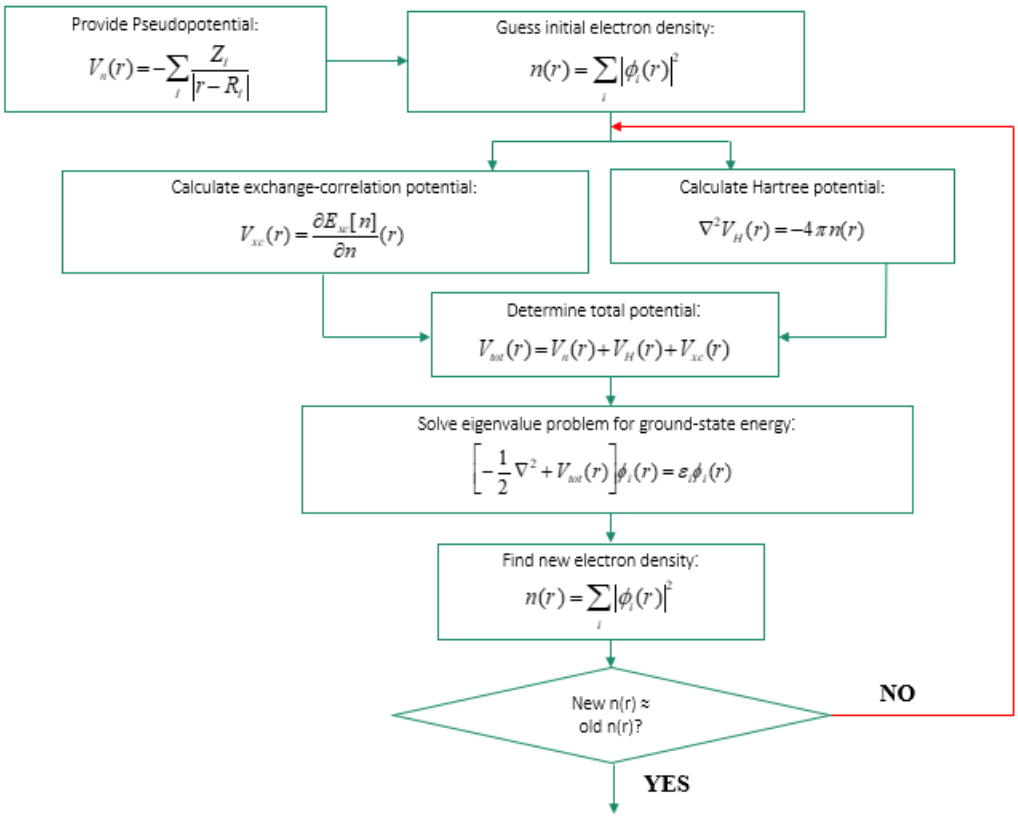

Figure 1.7: Schematic flow diagram for finding the self -consistent solutions for Kohn-Sham equations

1.4.8 Pseudopotentials

Pseudopotentials or effective potentials are used to describe the complex systems in a simplified approximation. The complicated effects of the motion of the core electrons of an atom are replaced with an effective potential. This approach uses effective potential term instead of a Coulombic potential term for the core electrons in the Schrödinger equation.

The pseudopotential is constructed in way that the atomic all-electron potential that describes the core states are eliminated and the valence electrons are described pseudo-wavefunction with significantly lower nodes, thus making the basis set used more practical. In this approach only the chemically balanced valence electrons are dealt with explicitly while the core electrons are assumed to be fixed, by considering them together with the nuclei (together as ion core). First-Principle pseudopotentials are derived from an atomic reference state, provided the pseudo-eigenstates and all electron eigenstates have the same energies and amplitude outside a core cut-off radius, r_c.

Pseudopotentials with large cut-off radius are softer, i.e. they converge more rapidly. These softer pseudopotentials are however less transferable meaning they are less accurate to reproduce the realistic features of ionic interactions in different environments.

Effective potentials are used in order to reduce the size of the basis set used, reducing the number of electrons and include all other effects. The most common types of pseudopotentials are norm-conserving pseudopotentials and ultra-soft pseudopotentials.

1.4.8.1 Norm-conserving Pseudopotentials

Norm-conserving pseudopotentials allow a basis-set with a significantly lower cut-off to be used to describe the electron wavefunctions. This allows a proper numerical convergence with reasonable computing resources. Norm-conserving pseudopotential is of the form [48]:

$$\hat{V}(r) = \Sigma_l \Sigma_m \left| Y_{lm} \right\rangle V\_lm\ (r) \left\langle Y_{lm} \right| \tag{43}$$

Where $\left| Y_{lm} \right\rangle$ projects the one-particle wavefunction to the angular momentum labeled by $\{l, m\}$. $V_{lm}(r)$ is the pseudopotential that acts on the projected component. Different angular momentum states feel different potentials. Therefore, the norm-conserving pseudopotential is non-local.

Inside the cut-off radius, r_c, the norm of each pseudo-wavefunction will be identical to its corresponding all-electron wavefunction [58]:

$$\int_{r<r_c} dr^3 \phi_{R,i}\,(\vec{r}) \phi_{R,j}(\vec{r}) = \int_{r<r_c} dr^3 \tilde{\phi}_{R,i}\,(\vec{r}) \tilde{\phi}_{R,j}(\vec{r}) \tag{44}$$

Where $\phi_{R,i}$ &$\phi_{R,j}$ are the all electron and pseudo reference states for the pseudopotential on atom R. All electron and pseudo-wavefunctions are identical outside cut-off radius, r_c.

1.4.8.2 Ultra-soft Pseudopotentials

Ultra-soft pseudopotentials relax the norm-conserving constraint to reduce the necessary basis set size further at the expense of introducing a generalized eigenvalue problem. With the non-zero difference in norms we can now define [48]:

$$q_{R,ij} = \langle \phi_{R,i} | \phi_{R,j} \rangle - \langle \tilde{\phi}_{R,i} \left| \tilde{\phi}_{R,j} \right\rangle \tag{45}$$

So, a normalized eigenstate of the pseudo-Hamiltonian obeys the generalized equation,

$$\widehat{H}\left|\Psi_i\right\rangle = \varepsilon_i \hat{S}\left|\Psi_i\right\rangle \tag{46}$$

Where, the operator $\hat{S}$ is defined as

$$\hat{S} = 1 + \Sigma_{R,ij}\left|p_{R,i}\right\rangle q_{R,ij}\left\langle p_{R,ij}\right| \tag{47}$$

Where, $p_{R,i}$, are the projector that form dual basis with the pseudo reference states inside the cut-off radius, and zero outside.

$$\langle p_{R,i}|\tilde{\phi}_{R,j}\rangle_{r<r_c} = \delta_{i,j} \tag{48}$$

QuantumATK has a variety of norm-conserving pseudo potentials and ultra-soft pseudopotentials built into the tool. Having learnt about the basics of DFT that involves solving the standard one particle Schrödinger equation defined by Kohn-Sham equations that uses accurate and simple exchange correlation energy functionals, that includes all many body principle effects, we now dive into applying these DFT calculations on CdTe bulk structure using QuantumATK, in order to obtain structural and electronic properties of CdTe, which is the primary focus of this thesis.

CHAPTER 2: CALCULATING CRYSTAL STRUCTURE OF CdTe USING QUANTUM ATK

2.1 Introduction to QuantumATK

QuantumATK (Atomistix Tool Kit) is an integrated set of atomic-scale modelling tools developed by professional software engineers in collaboration with academic researchers. The simulation engines included in the QuantumATK platform enable electronic-structure calculations using density functional theory. It has complete set of tools for atomistic simulations. The benefit of QuantumATK is its Graphical User Interface (GUI), called Virtual Nano Lab (VNL). It is simple and very user friendly. VNL can be used as GUI for other codes because we can import many kinds of filetypes and export them to use in other programs. QuantumATK can model the electronic properties of closed and open quantum systems within the framework of DFT. It uses numerical Linear Combination of Atomic Orbitals (LCAO) basis sets. The key parameter in the self-consistent calculation of the Kohn-Sham equations is the density matrix, which defines electron density. For open systems, the tool uses non-equilibrium Green's functions (NEGF's) for calculating the density matrix and for the closed system the density matrix is calculated using diagonalization of the Kohn-Sham Hamiltonian. The NEGF functions are suited when studying the interfaces, while diagonalization technique can be used for the atoms, molecules and crystal structures. The calculated electron density then sets up an effective potential, which is given by the Hartree, external and exchange-correlation potentials.

QuantumATK platform offers simulation engines covering entire range of atomic-scale simulation methods relevant to the semiconductor industry and material sciences in general. This platform provides a large suite of exchange-correlation functionals. LDA, GGA, MGGA and

Hybrid functionals are mainly supported by the tool. Also, ATK uses norm-conserving pseudopotentials to avoid explicit DFT calculations of core electrons and includes a database of pseudopotentials for all the elements in the periodic table. The default pseudopotentials in QuantumATK are SG15 and PseudoDojo [59]. We use SG15 pseudopotential type with GGA exchange-correlation functional (semi-local) and PseudoDojo with LDA exchange-correlation functional (local) in our process of calculating properties of CdTe. For Each pseudopotential QuantumATK generates an optimized LCAO basis set.

2.1.1 Linear Combination of Atomic Orbitals (LCAO) Representation

QuantumATK uses the DFT-LCAO method for the numerical representation of the Kohn-Sham equations. In DFT-LCAO method, the single electron eigen functions, Ψ_α, are expanded in a set of finite-range atomic-like basis functions ϕ_i,

$$\Psi_\alpha(r) = \Sigma_i C_{\alpha i}\phi_i(r) \tag{49}$$

$C_{\alpha i}$ are the expansion coefficients that are determined by representing the Kohn-Sham equation as a matrix equation given below.

$$\Sigma_j H_{ij}^{KS} C_{\alpha j} = \varepsilon_\alpha \Sigma_j S_{ij} C_{\alpha j} \tag{50}$$

$H_{ij}^{KS} = \langle\phi_i|\widehat{H}^{KS}\rangle\phi_j$ is the Hamiltonian matrix, and $S_{ij} = \langle\phi_i \,|\, \phi_j\rangle$ is the overlap matrix. The matrices are represented by the integrals with respect to the electron coordinates. Two-center integrals are computed using one-dimensional radial integration employing a Fourier transform technique, while the multiple-center integrals are computed on a real-space grid [61].

Now, density matrix D_{ij}, is determined by diagonalization of Hamiltonian matrix in molecules and bulk systems.

$$D_{ij} = \Sigma_{\alpha} C_{\alpha i}^{*} C_{\alpha j} . f\left(\frac{\varepsilon_{\alpha} - \varepsilon_{F}}{k_B T}\right) \quad (51)$$

Where f is the Fermi-Dirac distribution of electrons over energy states, ε_F the Fermi energy, T the electron temperature, k_B the Boltzmann constant.

The electron density is given by,

$$n(r) = \Sigma_{ij} D_{ij} \phi_i(r) \phi_j(r) \quad (52)$$

Using this electron density, we calculate the total energy of the system by solving the Kohn-Sham Schrödinger equation (E[f(n)]) [60].

2.1.2 Plane-Wave (PW) Representation

Bulk systems with periodic boundary conditions are simulated using the ATK-Planewave engine. The Kohn-Sham eigenfunctions are expanded in terms of Plane-wave basis functions.

$$\Psi_{\alpha}(r) = \Sigma_{|g|<g_{max}} C_{\alpha}, g^{e^{ig.r}} \phi_i(r) \quad (53)$$

Where g are reciprocal lattice vectors. g_{max} is the upper threshold for the reciprocal lattice vector length and in plane-wave expansion is determined by a kinetic energy cutoff, E_{cut}

$$\frac{\hbar^2 g_{max}^2}{2m} < E_{cut} \quad (54)$$

The DFT-PW approach has distinct advantages and disadvantages compared to the DFT-LCAO approach. Using plane-wave expansion of Kohn-Sham eigenfunctions is computationally

efficient for small bulk systems. The obtained physical quantities can be systematically converged with respect to the basis set size by increasing the kinetic energy cutoff. However, the plane-wave representation is not computationally efficient for low-dimensional systems with large vacuum regions [60].

2.2 Methods used for Predicting the Crystal Structure for CdTe

We can perform DFT calculations, using QuantumATK, to calculate the crystal structure of CdTe. So, prior to calculating any structural properties, the interest was to see, what crystal structure does QuantumATK predicts for CdTe? The crystal structure of CdTe is already known from the experiment. However, in general we might not know the most stable state of CdTe crystal lattice. In this case the optimization procedure was repeated for, the Simple Cubic lattice (SC), Body Centered Cubic (BCC) and Face Centered Cubic (FCC) because the CdTe crystal is known to be a cubical structure from experiment [47]. This stable state was compared by calculating the total energy values around the experimental lattice parameter range (approx. 6.5Å). Also, this approach was done using two different exchange correlation functionals LDA and GGA.

In Quantum ATK, builder tool was used for constructing a desired crystal lattice configuration for CdTe. Initially, the SC geometry was constructed using the primitive lattice vectors represented as, $a_1 = au_x$, $a_2 = au_y$ & $a_3 = au_z$, where a is the lattice parameter. The Cd atom occupies the position at origin and the Te atom occupies $(\frac{1}{4},\frac{1}{4},\frac{1}{4})$. Similarly, the BCC geometry was built using the primitive lattice vectors $a_1 = \frac{1}{2}a(u_x + u_y - u_z)$, $a_2 = \frac{1}{2}a(-u_x + u_y + u_z)$& $a_3 = \frac{1}{2}a(u_x - u_y + u_z)$ and repeated for FCC using primitive lattice

vectors $a_1 = \frac{1}{2}a(u_x + u_y)$, $a_2 = \frac{1}{2}a(u_y + u_z)$, $a_3 = \frac{1}{2}a(u_x + u_z)$. Crystal structure optimizations were done for these crystals on ATK-DFT tool for using exchange correlation functionals (LDA, GGA) to see what structures they predict. The Cd atom has atomic number 48 and the electronic configuration **1s2 2s2 2p6 3s2 3p6 4s2 3d10 4p6 5s2 4d10,** and the Te atom has atomic number 52 with a configuration **1s2 2s2 2p6 3s2 3p6 4s2 3d10 4p6 5s2 4d10 5p4**. The core electrons are assumed to be fixed to the nuclei of Cd and Te atoms respectively and their effects are taken into consideration using by pseudopotentials (PseudoDojo and SG15 in the calculations below). So, only valence electrons of Cd (**5s2 4d10**) and valence electrons of Te (**4d10 5p4**) and the DFT calculations will only involve two nuclei and 26 electrons.

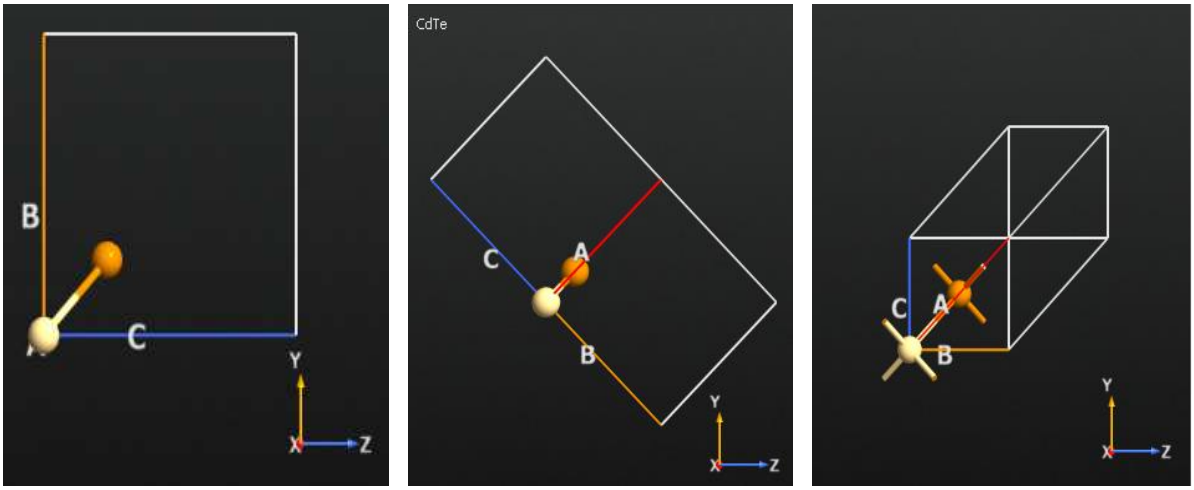

Figure 2.1: Primitive cells of possible CdTe crystal lattice compared, a) Simple Cubic b) BCC c) FCC.

2.2.1 Crystal lattice comparison using LDA

To apply ATK-DFT calculations on the structures to perform optimization procedure, firstly K points were varied by having the density mesh cut-off (in eV) at a default value. Once the number of K points are converged within the specified tolerance, $10^{-3}eV$ was used as tolerance, then the calculated K points were used to converge the density mesh cutoff. With both converged K points and density mesh cutoff values, the lattice parameter values were varied to plot the total energy (in eV) vs lattice parameter (in Å). The exchange and correlation functional was selected as LDA and pseudopotential was as PseudoDojo using the script generator in QuantumATK. This process is repeated for all the three crystal structures and the figure (2.2) shows the comparisons of the crystal structure using the ATK-DFT calculations with LDA functional. The Kohn-Sham wavefunctions were expanded using the LCAO basis set in LCAO calculator in the script generator.

QuantumATK uses python script to run these calculations. The log files were generated for each iteration. The resultant total energy values are obtained and compared to see the most stable structure. The crystal structure with least total energy is considered to be the most stable structure at its ground state.

2.2.2 Crystal lattice comparison using GGA

The number of K-points and density mesh cutoff were obtained in similar method used in the above section for all the three crystal structures under consideration (SC, BCC, FCC). However, the exchange and correlation functional was selected as GGA and pseudopotential was as PseudoDojo using the script generator in QuantumATK. The comparisons of the crystal

structure using the ATK-DFT calculations with GGA functional are shown in the figure (2.3). The Kohn-Sham wavefunctions were expanded using the LCAO basis set in LCAO calculator in the script generator. The log files were generated for each iteration. The resultant total energy values are obtained and compared to see the most stable structure. The crystal structure with least total energy is considered to be the most stable structure at its ground state. The values obtained by GGA vary with LDA because the exchange energy in the low density/high density gradient region is restricted by no fundamental physical condition, the exchange functional forms in these regions have been determined to improve the reproducibility's of properties for CdTe.

2.3 Methods used for calculating lattice parameter of CdTe

To calculate the properties of CdTe at the surfaces using ATK-DFT, we need to find how ATK-DFT predicts the properties of CdTe bulk structure. Since typical crystal samples used in experiments contain billions of replicas of the basic crystal unit cell, it is advantageous to model the system as an infinite repetition of this periodic unit. Using this strategy, the Kohn-Sham equations were solved inside one periodic unit cell instead of dealing with a large crystal sample. The solutions within one unit cell is then matched to the equivalent solution on all other cells by imposing periodic boundary conditions. In the unit cell we expand the Kohn-Sham wavefunctions and the electron density using Fourier series.

At ambient conditions CdTe crystallizes into Zinc Blende, consisting of Face Centered Cubic (FCC) primitive lattice. The primitive lattice vectors are represented as, $a_1 = \frac{1}{2}a(u_x + u_y)$, $a_2 = \frac{1}{2}a(u_y + u_z)$, $a_3 = \frac{1}{2}a(u_x + u_z)$, with a the lattice parameter. The face centered cubic primitive cell consists of two atoms, one Cadmium (Cd) and one Tellurium (Te), at the positions

$R_{Cd} = (0,0,0)$ & $R_{Te} = (\frac{1}{4},\frac{1}{4},\frac{1}{4})$ with Rhombic Dodecahedron geometry. All the other atoms are generated by translations of this basis using linear combination of the primitive lattice vectors. Since, the primitive lattice vectors and atomic coordinates of the basis depend solely on the lattice parameter, a, the total potential energy will be function of this parameter. So, we can write the cohesive energy of CdTe as,

$$E_c(a) = \frac{V_{tot}(a)}{M} - E_{Cd} - E_{Te} \quad (55)$$

Where M is the total number of atoms in the crystal, $\frac{V_{tot}(a)}{M}$ is the potential energy per CdTe atom, and E_{Cd}, E_{Te} are total energy of an isolated Cd and Te atoms respectively. Equation (55) gives the information on how stable the CdTe crystal structure is relative to the collection of isolated atoms. The cohesive energy reaches zero as the lattice parameter increases to larger values. The DFT calculations will only involve two nuclei and 26 electrons, as the effects of the core electrons are replaced using an effective potential or pseudopotential.

Firstly, the LDA exchange and correlation functional and PseudoDojo pseudopotential were used to calculate the lattice parameter for FCC crystal structure of CdTe using the script generator. K points were varied by having the density mesh cut-off (in eV) at a default value. Once the number of K points are converged within the specified tolerance, $(10^{-3}eV)$ then the calculated K points were used to converge the density mesh cutoff. With both converged K points and density mesh cutoff values the lattice parameter values were varied to plot the total energy (in eV) vs lattice parameter (in Å). The exchange and correlation functional was selected as LDA and pseudopotential was as PseudoDojo using the script generator in QuantumATK. Figure (2.4) show the plots for the K points convergence and density mesh cutoff convergence using LDA and figure (2.5) show the plot for Total energy vs Lattice parameter, from which the lowest energy value and

the lattice parameter associated with it is calculated. These calculations were repeated using GGA and Meta-GGA exchange correlation functionals using SG15 pseudopotential. Table 2.1 shows the calculated lattice parameter values for CdTe using LDA, GGA, MGGA functionals and their comparisons with experimental value for lattice parameter of CdTe.

2.4 Results and Discussions

2.4.1 Crystal structure predicted

The crystal lattice with the least total energy value at the equilibrium is known to be the most stable form in its ground state. After performing the calculation using ATK-DFT it was observed that FCC crystal lattice was more stable, because the total energy is least for this lattice.

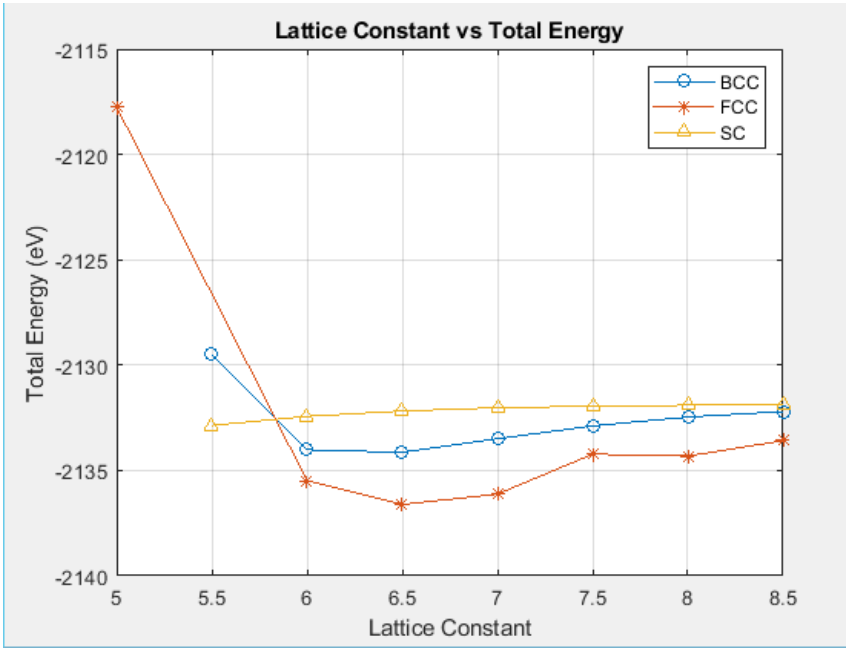

Figure 2.2: Total Energy vs Lattice parameter using LDA functional to compare possible cubic structures for CdTe.

Figure (2.5) shows the plot for Energy vs lattice parameter (in Å) using LDA and the Figure (2.7) shows the plot for Energy vs lattice parameter (in Å) using GGA. From the both the plots, it can be seen that the total energy values for the FCC lattice are the least.

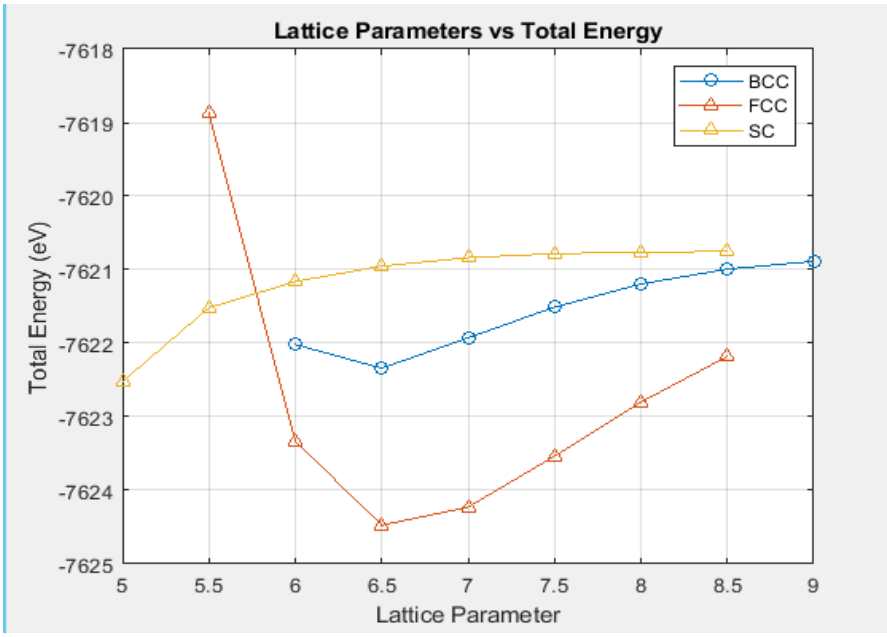

Figure 2.3: Total Energy vs Lattice parameter using GGA functional to compare possible cubic structures for CdTe.

The QuantumATK using LDA and GGA exchange correlation functionals correctly determines the preferred CdTe Zinc-blend structure. As we can also see from the plot the total energy tends to increase beyond lattice constant value 6.5 Å, which agrees the equation (55), which the total energy tends to approach zero for the CdTe system as the distance between the atoms is increased to the larger numbers.

If we look into the plots, the energy values obtained using LDA are close for all the crystal lattices. It is acceptable because the LDA functional uses just the local density as a functional of energy. So, the crystal lattices considered for CdTe have close local densities for the three crystals

because of same number of nuclei and electrons used. While the energy values calculated using the GGA have large difference among the SC, BCC and FCC crystal lattices because the GGA functional consider the local density and the gradient of it in both low density and high density regions. When other accurate exchange-correlation functionals are used we can see higher differences in the values obtained. However, the trade-off those functionals is they have high computational costs and times.

2.4.2 Lattice parameter obtained using different exchange-correlation functionals

For the correctly predicted Zinc-blend structure of CdTe using QuantumATK, the next step was to calculate the lattice parameter of CdTe using different exchange-correlation functionals and compare the values obtained with the experimental value.

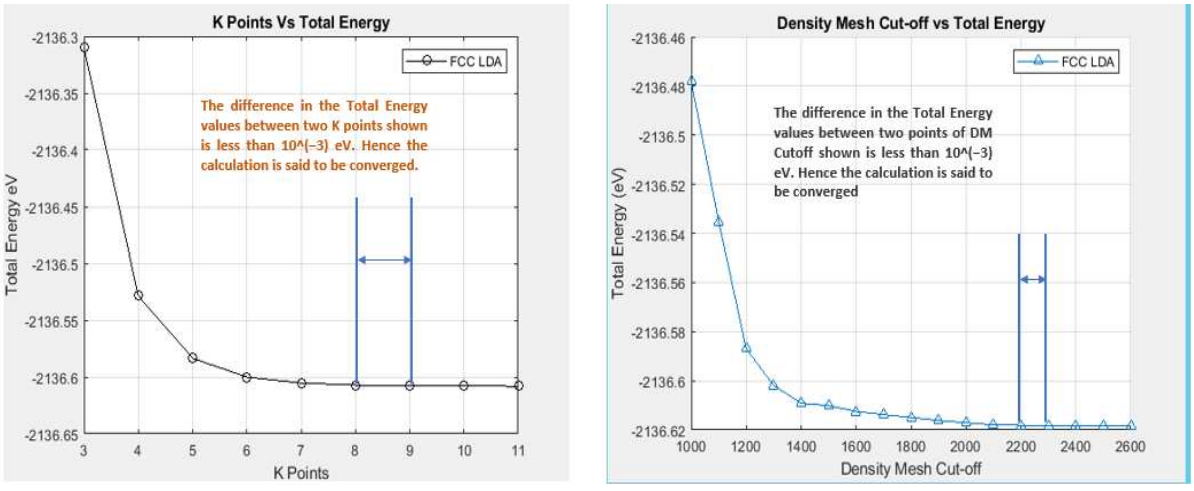

Figure 2.4: Convergence of K points (left) and density mesh cutoff (right) using LDA functional for CdTe FCC Structure.

In the plot the total energy vs k-points, the total energy varies decreases greatly by increasing the k-points. At certain number of k-points the change in energy is slow and the

difference between total energy values between two k points is less than the allowed tolerance. Therefore, the k-points are said to be converged. The calculations show that the k-points are well converged between points 9 and 10. The total energy value obtained at (10X10X10) sampling points is -2136.60810 eV and compared to the -2136.60802 eV at (9X9X9). The difference in the energy between these two sampling points is $-8x10^{-4}$ eV. The density mesh cutoff value convergence is calculated using (10X10X10) sampling points in the reciprocal space. The plot shows that the density mesh cutoff has converged between 2200 eV and 2300 eV. The total energy values calculated for density mesh cutoffs at 2200eV are -2136.60816 eV and at 2300 eV it is -2136.60816 eV where the difference is zero eV. The lattice parameter of CdTe is now calculated using these converged values for k-points and density mesh cutoffs (10X10X10 and 2300 eV).

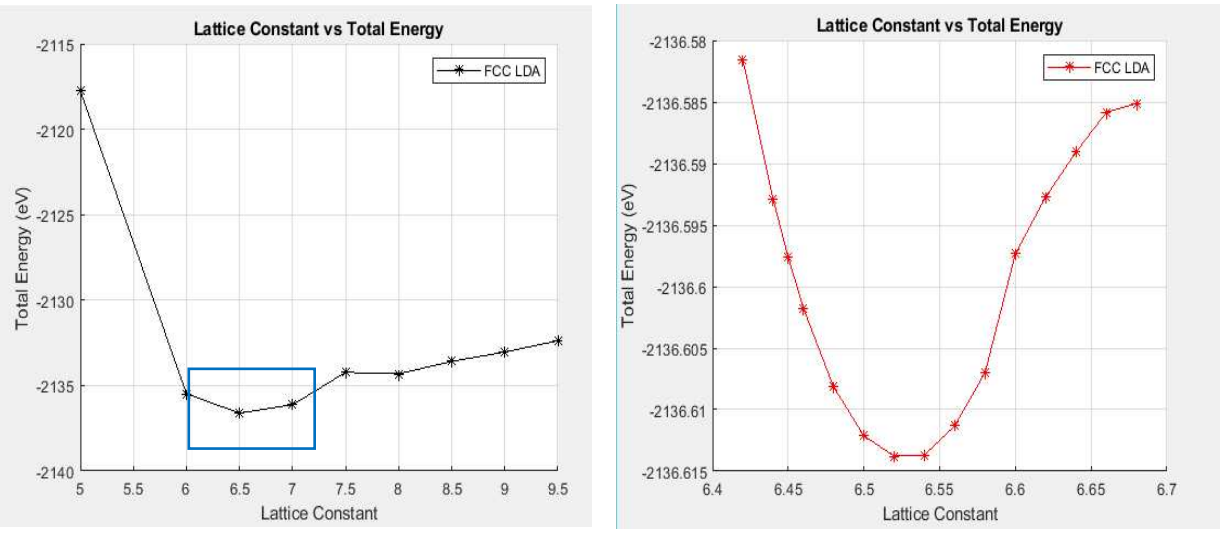

Figure 2.5: Lattice constant Å vs total energy using LDA functional for CdTe FCC Structure.

The plot in figure (2.5) shows that the total energy of the CdTe bulk structure (FCC crystal structure) is least in between 6.5 to 7 Å. Further investigation was done in between these two lattice

parameter values and the second plot in the figure (2.5) shows the total energy for that range. From the plot we can see that the ATK-DFT using LDA exchange-correlation functional the lattice parameter is 6.548 Å and the energy value at that point is -2136.61378 eV. The experimental value for the lattice parameter for CdTe bulk structure in FCC is 6.482 Å [73]. The calculated value of lattice parameter using LDA is only overpredicts it by 1.02%, which is an acceptable error percentage.

Similarly, the lattice parameter obtained using GGA exchange-correlation functional is discussed below.

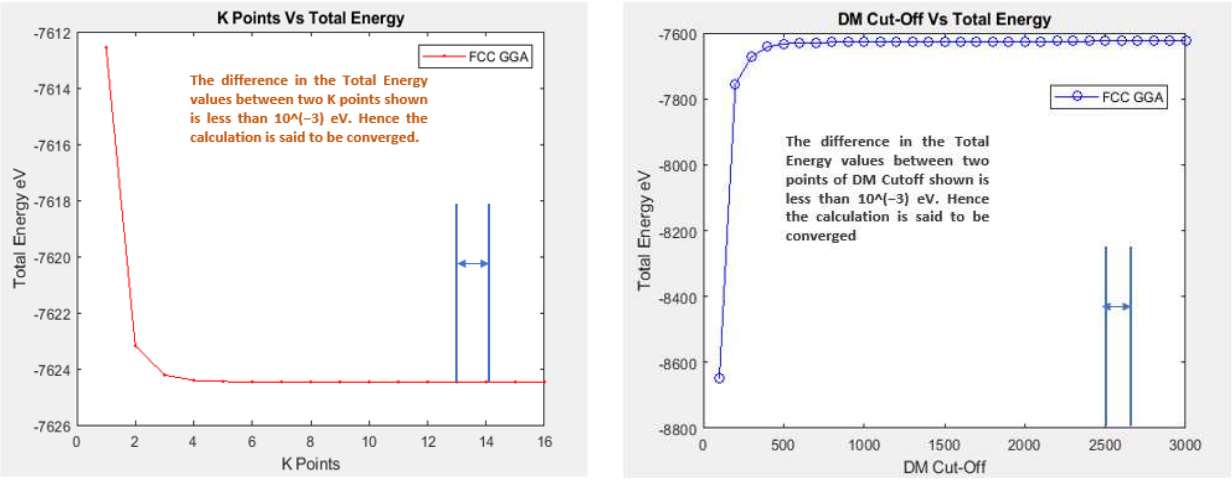

Figure 2.6: Convergence of K points (left) and density mesh cutoff (right) using GGA functional for CdTe FCC Structure.

The k-points are converged between 12 and 13 points using GGA functional. The energy values at (13X13X13) and (12X12X12) are -7624.47342 eV and -7624.47336 eV respectively. The difference in the energy between these two sampling points is $-6x10^{-4}$ eV which is less than the allowed tolerance. Using (13X13X13) sampling points the density mesh cutoff was converged between 2500eV and 2600 eV. The energy value at these cutoffs were -7624.46402 eV and

-7624.46413 eV respectively. The density mesh cutoff value of 2600 eV is used to calculate the lattice parameter.

All the y axis energy is dependent on the $V_n, and\ V_{xc}$ terms of the Kohn-Sham equations that vary with different exchange-correlation functionals and pseudopotentials used.

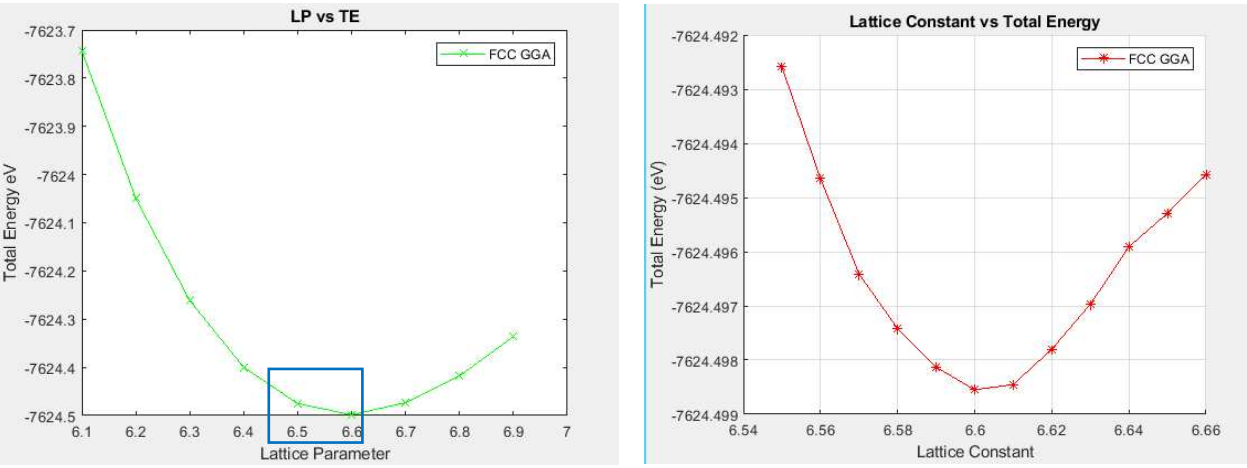

Figure 2.7: Lattice constant Å vs total energy using GGA functional for CdTe FCC Structure.

From the plot we can see that the ATK-DFT using GGA exchange-correlation functional the lattice parameter is 6.614 Å and the energy value at that point is -7624.49591 eV. When compared to the experimental value of the lattice parameter (6.482 Å) [73] the GGA functional overpredicts it by 2.18%, which is close but not better than LDA. The reason for this can be implicitly related to the density gradient in lower density and higher density regions used by the GGA functional.

Finally, the k-points are convergence using MGGA is calculated between 10 and 11 sampling points. The energy values at (10X10X10) and (11X11X11) are -7706.84260 eV and -7706.84260 eV respectively. The difference in the energy between these two sampling points is $-5x10^{-4}$ eV which is less than the allowed tolerance. The density mesh cut for MGGA

calculations converge between 2700 eV and 2800 eV with energy values -7706.82631 eV and -7624.82631 eV respectively, where the difference in energy is zero eV. The density mesh cutoff value of 2800 eV is used to calculate the lattice parameter.

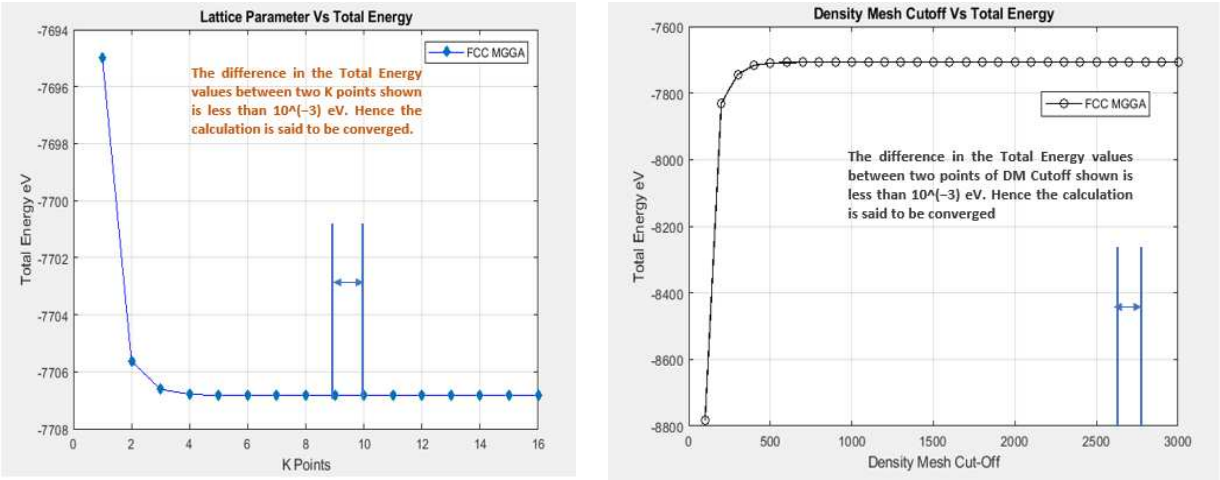

Figure 2.8: Convergence of K points (left) and density mesh cutoff (right) using MGGA functional for CdTe FCC Structure.

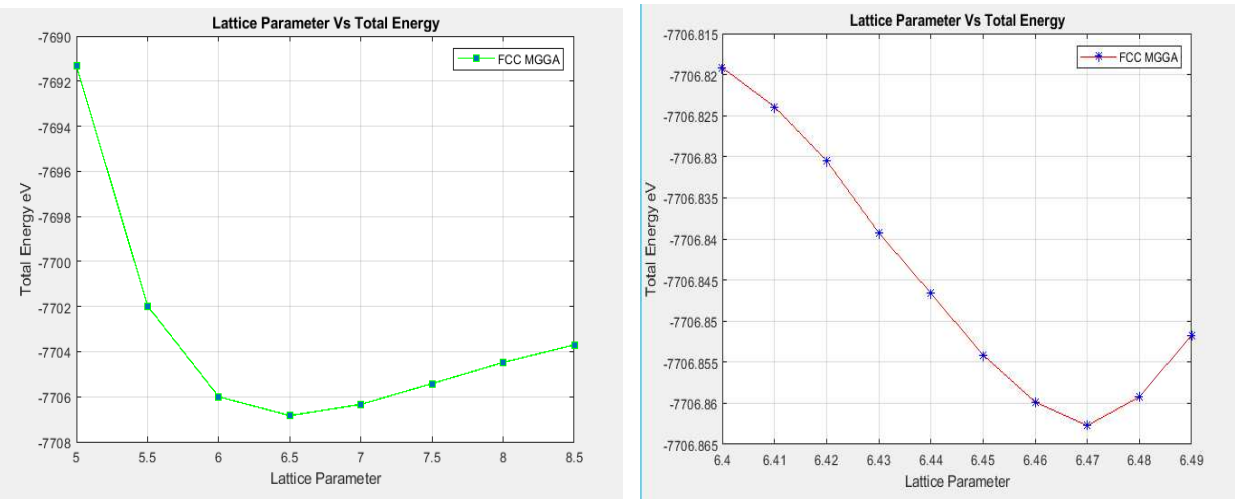

Figure 2.9: Lattice constant Å vs total energy using MGGA functional for CdTe FCC Structure.

From the figure (2.9) we can see that the ATK-DFT using MGGA exchange-correlation functional the lattice parameter is 6.477 Å and the energy value at that point is -7706.84072 eV. When compared to the experimental value of the lattice parameter (6.482 Å) [73] the lattice

parameter calculated using MGGA functional is smaller by 0.08%, which is very close compared to the three exchange-correlation functionals used and the errors of these margins are very likely accepted while computing crystal structure properties. Table 2.1 summarizes the comparison of the lattice parameter values calculated using different exchange-correlation functionals in this experiment using QuantumATK to the experimental values and the percentage of deviation to the experimental value is also shown.

Table 2.1: Comparison of calculated lattice parameters using different exchange-correlation functionals with experimental value.

Method Used	**Lattice Parameter in Å**	**Percentage Error %**
Experiment	6.482	-
LDA	6.548	1.02
GGA	6.614	2.18
MGGA	6.477	0.08

Clearly MGGA calculates the lattice parameter close to the experimental value. This is because the MGGA includes the correction for the difference between kinetic energy of non-interacting electrons system and the kinetic energy of interacting electrons system which changes the total energy calculated and hence corrects the lattice parameter value. Whereas in GGA the difference in kinetic energy term is not included while LDA considers energy as the functional of local electron density alone. Therefore, LDA and GGA result in higher values of lattice parameter for CdTe compared to the experimental value resulting higher error percentages.

CHAPTER 3: CALCULATING BAND STRUCTURE OF CdTe USING QUANTUM ATK

3.1 Calculating Band Structure in Crystals using DFT

If we rewrite the equations (42),

$$\left[-\frac{1}{2}\nabla^2 + V_{total}(r)\right]\phi_i(r) = \varepsilon_i\phi_i(r)$$

$$V_{total}(r) = V_n(r) + V_H(r) + V_{xc}(r)$$

$\phi_i(r)$ in these equations are the Kohn-Sham (KS), wavefunctions, ε_i the corresponding eigenvalues and $V_{total}(r)$ is the effective potential experienced by the electrons [6]. This effective potential includes the nuclear contribution V_n , Hartree term V_H and the exchange and correlation term V_{xc}. The KS wavefunctions are used to build the electron density $n(r)$. However, these wavefunctions and eigenvalues are very useful to interpret the complex experimental data.

DFT electronic total energy from equation (28) can be expressed as:

$$E = \Sigma_i f_i \varepsilon_i - [E_H + \int dr\, V_{xc}(r)n(r) - E_{xc}] \quad (56)$$

Where $f_i = 1$ for the occupied KS states, and 0 for unoccupied states [6]. The sum of the energies of all the occupies KS states is referred to as the band structure energy (the first term in equation (56). The band structure term already contains twice the Hartree energy and exchange-correlation energies. Therefore, these terms must be subtracted as shown in the equation (56) to avoid double counting. Now taking the partial derivatives of the total energy with respect to the occupations f_i, from equation (56)

$$\frac{\partial E}{\partial f_i} = \varepsilon_i \tag{57}$$

Equation (57) (derived originally by Janak [38]) implies that, in a system of N electrons with energy E_N, if we add or remove one electron in the unoccupied state ϕ_i, the resulting total energy can be denoted $E_{N+1,i}$. The change in total energy in this process is:

$$E_{N+1,i} - E_N = \int_0^1 df_i \frac{\partial E}{\partial f_i} = \int_0^1 df_i \, \varepsilon_i \tag{58}$$

However, in solids and large nano crystals, the number of electrons is so large that the change in density can be neglected. So, the equation (58) can be written as:

$$E_{N+1,i} - E_N \approx \varepsilon_i \tag{59}$$

This equation implies that, when one electron is added or removed to the solid, the total energy changes approximately by a value corresponding to the KS eigenvalue of the new electron. From this we can assume that each electron carries an energy corresponding to the eigenvalue of the KS state it occupies. To describe the eigenvalues and eigenstates in crystalline solid we use Bloch's theorem, which state that the single-particle wavefunction in a crystal can be expressed as the product of a function periodic in a unit cell and a plane wave. This periodic function is called Bloch function. The electronic wave function in a crystal can be written as:

$$\phi_i(r) = \phi_{ik}(r) = e^{ik.r} u_{ik}(r) \tag{60}$$

Where,

$$u_{ik}(r + T) = u_{ik}(r), \ \& \ T = n_1 a_1 + n_2 a_2 + n_3 a_3 \tag{61}$$

i, in the exponential term is a complex number, while i in $\phi_{ik}(r)$ is the eigenstate index [6]. On substituting the wavefunctions with the expression from equation (60) in equation (42) and

multiplying the exponential term on both sides and performing the second order derivative on the equation obtained, we can get the result:

$$\left[-\frac{1}{2}(\nabla + ik)^2 + V_{tot}(r)\right] u_{ik}(r) = \varepsilon_{ik} u_{ik}(r) \tag{62}$$

Equation (62) shows the KS equations for crystals and periodic part of the KS wavefunction is an eigenstate of a modified Hamiltonian.

$$\widehat{H}_k \, u_{ik} = \varepsilon_{ik} u_{ik} \tag{63}$$

&

$$\widehat{H}_k = -\frac{1}{2}(\nabla + ik)^2 + V_{tot} \tag{64}$$

A periodic model of a crystalline solid is infinitely extended, therefore, the function $u_{ik}(r)$ id normalized inside one unit cell of the crystal [68].

$$\int_{UC} |u_{ik}(r)|^2 dr = 1 \tag{65}$$

This is important because, in order to study electrons in crystals, we need to solve Schrödinger equation only inside one crystalline unit cell and apply periodic boundary conditions. $u_{ik}(r)$ determined in one unit cell is a replica of the function in any other crystal since it is periodic (equation (61)). This approach saves a lot of computational time and resources. The numerical solution for Schrödinger equation requires the description of u_{ik} on a discrete mesh of points forming one unit cell.

In a reciprocal space, the solutions for Hamiltonians $\widehat{H}_{k+G}$ (G is a reciprocal space vector), are simply duplicates of solution for $\widehat{H}_k$, and therefore, we can restrict the useful range of wavevectors k to the first Brillouin zone. This restriction will also avoid duplicate wavefunctions.

With the solutions for KS equations in crystal calculated, the electron density is constructed. The density can be calculated in the self-consistent method, by replacing $\phi_i(r)$ with $\phi_{ik}(r)$ and by taking summation over both indices, i and wavevectors k.

$$n(r) = \Sigma_i \int_{BZ} \frac{dk}{\Omega_{BZ}} f_{ik} |u_{ik}(r)|^2 \tag{66}$$

The electron density is also periodic from equation (66) with a periodicity u_{ik}. Therefore, the electron density is same in every unit cell. The total KS potential can be calculated using this electron density from:

$$E = \Sigma_i \int_{BZ} \frac{dk}{\Omega_{BZ}} f_{ik}\, \varepsilon_i - [E_H + \int dr\, V_{xc}(r) n(r) - E_{xc}] \tag{67}$$

Each energy term in the equation is the energy per unit cell. The Hartree potential and exchange-correlation potential are completely determined by electron density, the ground state of the system is obtained by choosing the occupation numbers that fill the states, starting from the lowest energy states. The electron density adds up to the number of electrons per unit cell.

$$N = \int_{UC} n(r) = \int_{BZ} \frac{dk}{\Omega_{BZ}} f_{ik} \tag{68}$$

The energy of highest occupied eigenstate at T=0 is referred to as Fermi-Energy level (ε_F). The total energy, E, is minimized when every KS state below the Fermi level is occupied and every state above the Fermi level is empty. The Brillouin zone integral in electron density equation is evaluated numerically by considering a discrete mesh of wavevectors k, spanning the Brillouin zone. The size of the mesh depends on the size of the crystal.

3.2 Band Structure of CdTe

With the knowledge of how the band structures in crystals are calculated in DFT, QuantumATK tool was used to calculate the band gap for CdTe. Different exchange-correlation functionals like LDA, GGA, MGGA, HSE06 were used in the process. Also, for the band gap problem that occurs in DFT with LDA and GGA functionals, an attempt was made to solve the problems using DFT-1/2 corrections (LDA-1/2 and GGA-1/2) [62].

Initially, the unit cell of CdTe in its stable Zinc-blend (FCC) structure was constructed using the builder tool in QuantumATK.

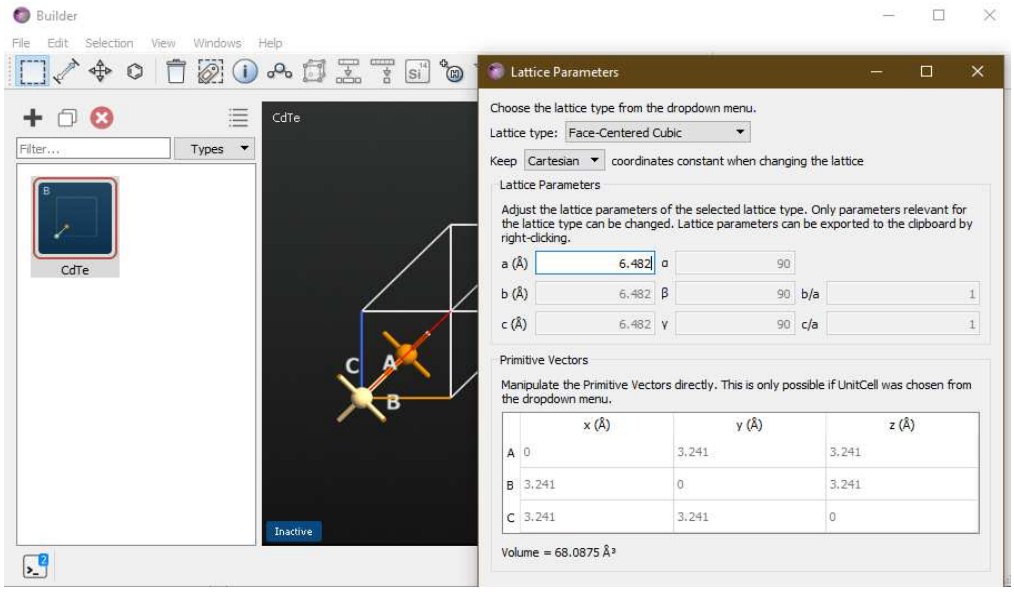

Figure 3.1: FCC unit cell built using Builder in QuantumATK.

The band structure using LDA functional was calculated first using the experimental lattice constant value (6.482 Å). The k-points mesh of 10x10x10 and density mesh cutoff 2300eV were used in these calculations. These values were obtained using optimization methods to converge

the calculations within desired tolerance, described during structural calculations. After the end of calculations using LDA functional the band gap of CdTe was analyzed using the band structure analyzer. The band gap values obtained are as shown in figure (3.6)

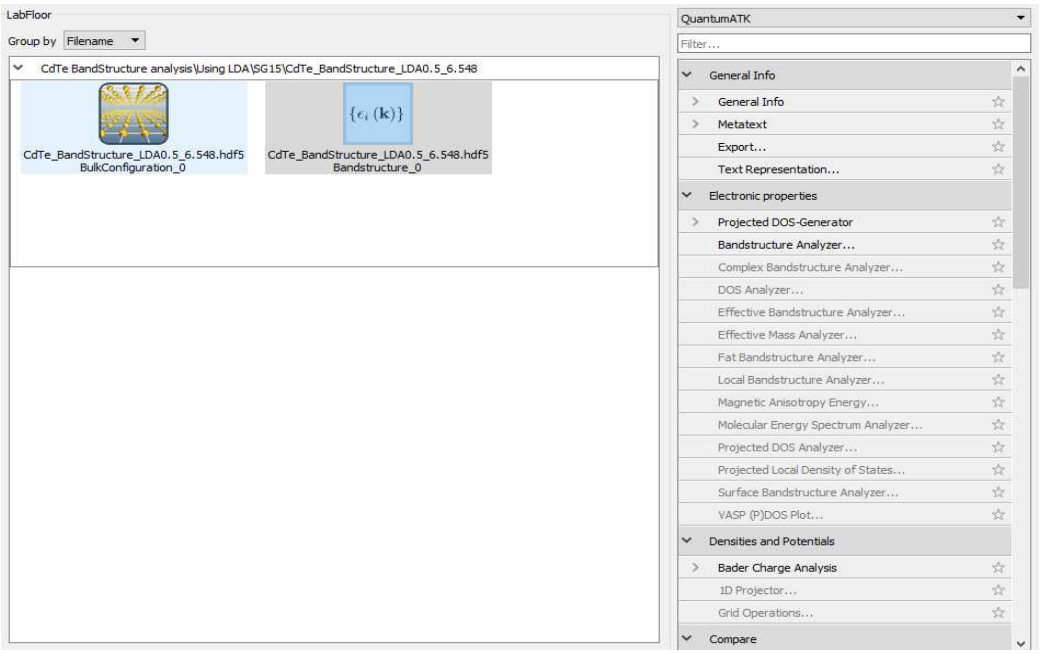

Figure 3.2: LabFloor of QuantumATK where the band structure of CdTe is analyzed.

Now, the calculations are repeated for GGA and MGGA functionals using the k-points and density mesh cutoff values obtained (converged) when the respective functionals were used. And the band gaps obtained are shown in figures (3.8) and (3.10) respectively.

The HSE06 hybrid functional used in the calculations uses planewave basis set to expand KS wavefunctions from which the density is calculated. The HSE06 hybrid functional extends the PBE exchange correlational functional by mixing the Hartree-Fock exchange integral only for the short-range part. This makes the Kohn–Sham energies of the independent electron model

link to those of the fully interacting electron one. The advantage of using QuantumATK is, we can also use plane wave basis set for the calculations. The HSE06 hybrid functional was applied using a planewave calculator. The k-points mesh, and wave function cutoff values used were 7x7x7 and 950 eV respectively. Note that the wave function cut off from the Hartree-Fock exchange term is used instead of density mesh cutoff on standard local and semi-local exchange -correlation functionals. The band gap for CdTe obtained using HSE06 hybrid functionals are shown in figure (3.12)

The band gap problem in DFT, can be solved using DFT-1/2 methods available in QuantumATK. It has low computational costs. To improve the LDA and GGA underestimations of the band gaps, LDA-1/2 and GGA-1/2 methods were employed. The aim of these methods is to remove the spurious electrostatic electron self-energy in the band structure calculations of CdTe (in crystals). This follows from Slater's transition technique. This idea is extended to crystals by adding an atomic self-energy potential to the crystalline potential. This self-energy is defined as the difference between the KS atomic potential and the potential of a system lacking half electron charge (-1/2 e). In case of semiconductors, only the anionic self-energy potential is important, because the valence band, composed mostly of anion states, is more localized than the conduction band. Therefore, it is more disrupted by its large self-energy. Band gaps calculated using different exchange-correlation functionals are discussed in the following section.

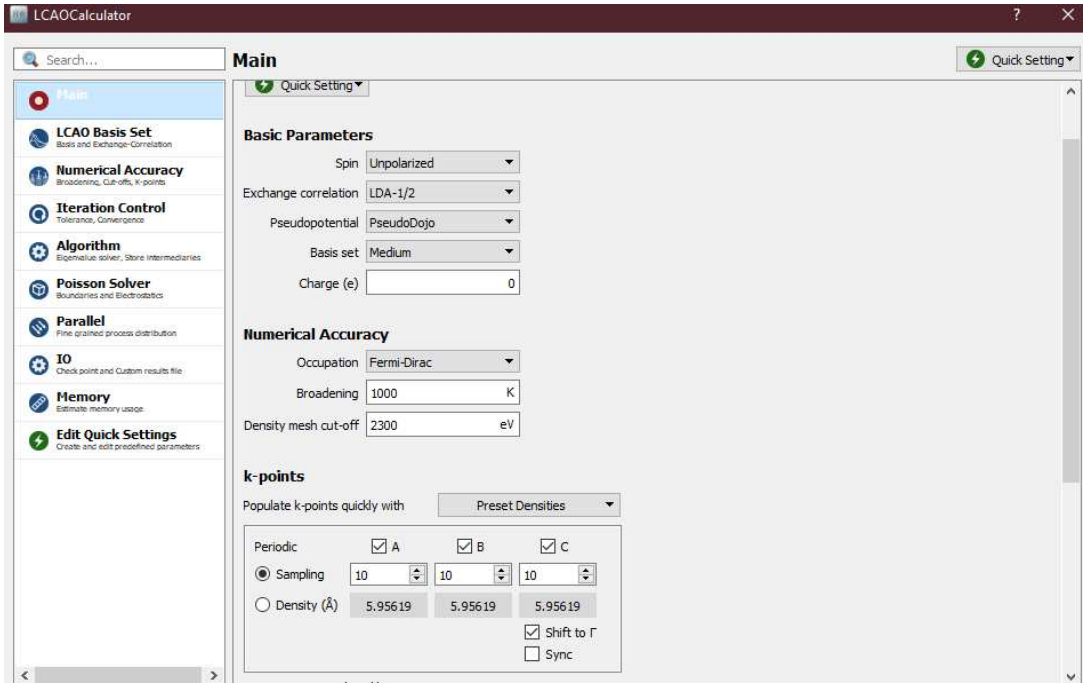

Figure 3.3: LDA-1/2 exchange-correlation used to correct the band gap prediction by LDA.

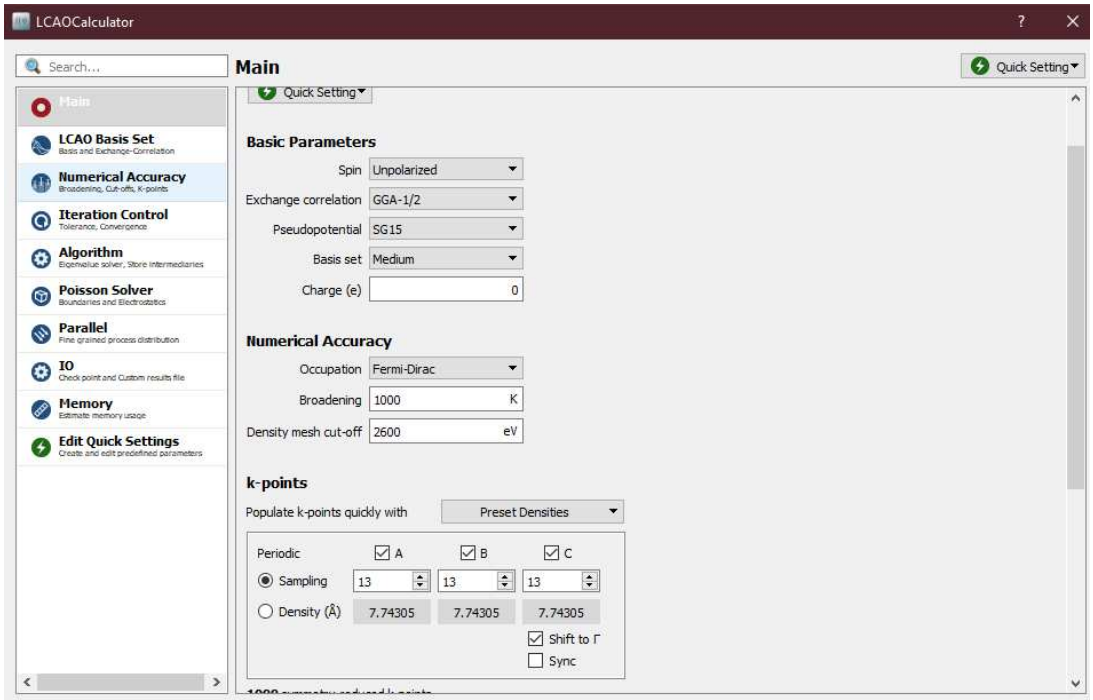

Figure 3.4: GGA-1/2 exchange-correlation used to correct the band gap prediction by GGA.

3.3 Results and Discussions

3.3.1 Band gaps determined by LDA and GGA

The valence electrons (26) of the CdTe are considered in the crystalline unit cell. Figure (3.5) shows the ε_{ik}, versus, wavevector k, dispersion relations of CdTe. The first step in calculating the band gap is to determine the electron density, $n(r)$ and the associated KS potential, $V_{tot}(r)$, which will define the KS Hamiltonian. The wavevector, k, is swept across the first Brillouin zone and for each wave-vector, the KS Schrödinger equation is solved to determine the eigenvalues $\varepsilon_{ik}, i = 1,2,3,$ .... The electron density and the total potential are left unchanged while determining the eigenvalues. Therefore, this step is known as non-self-consistent calculation. Which means we calculate the eigenvalues and eigenfunctions of the Schrödinger equation with the effective potential value as a known term. When the discrete eigenvalues calculated for each wave-vector along the given path are joined together, a continuous dispersion plot emerges. The plot obtained with all the bands (occupied energy states) is called band structure.

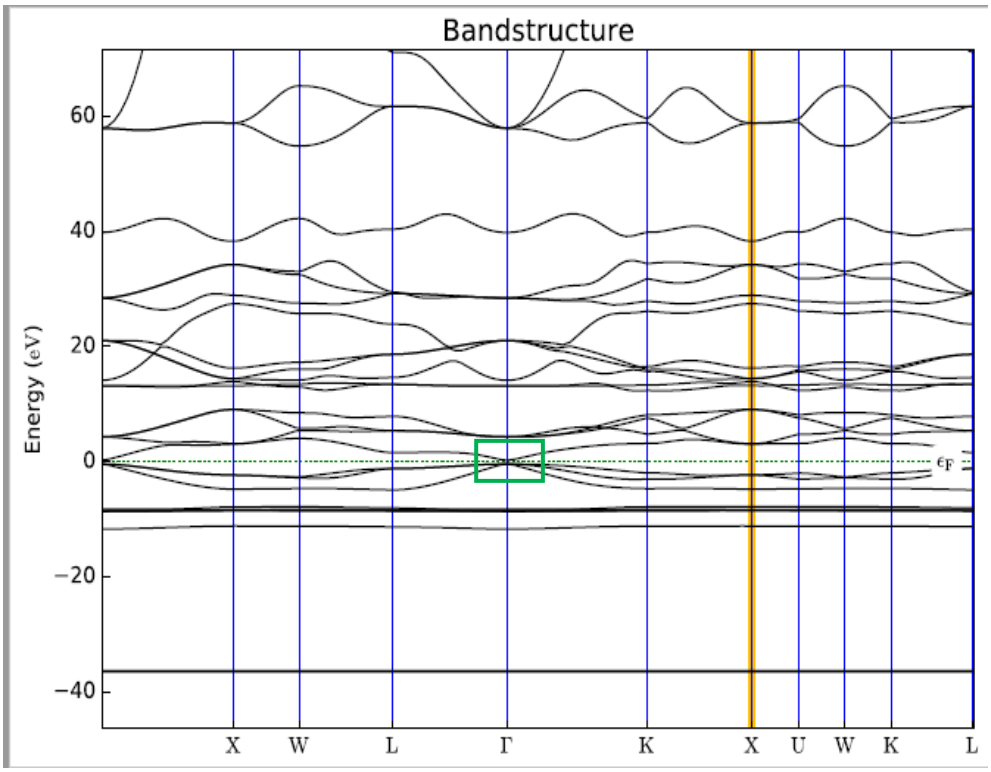

Figure 3.5: Electronic Band structure of CdTe obtained using LDA.

The Kohn-Sham eigenvalues are plotted along the typical high-symmetry paths of the CdTe Brillouin zone. The curves inside the figure (3.5) indicates the occupied states and the green dotted lines represent the Fermi-Energy level. If the image is zoomed (highlighted green box) in the region, then we can see the energy difference between the conduction band minimum and valence band maximum i.e. the band gap value obtained using LDA.

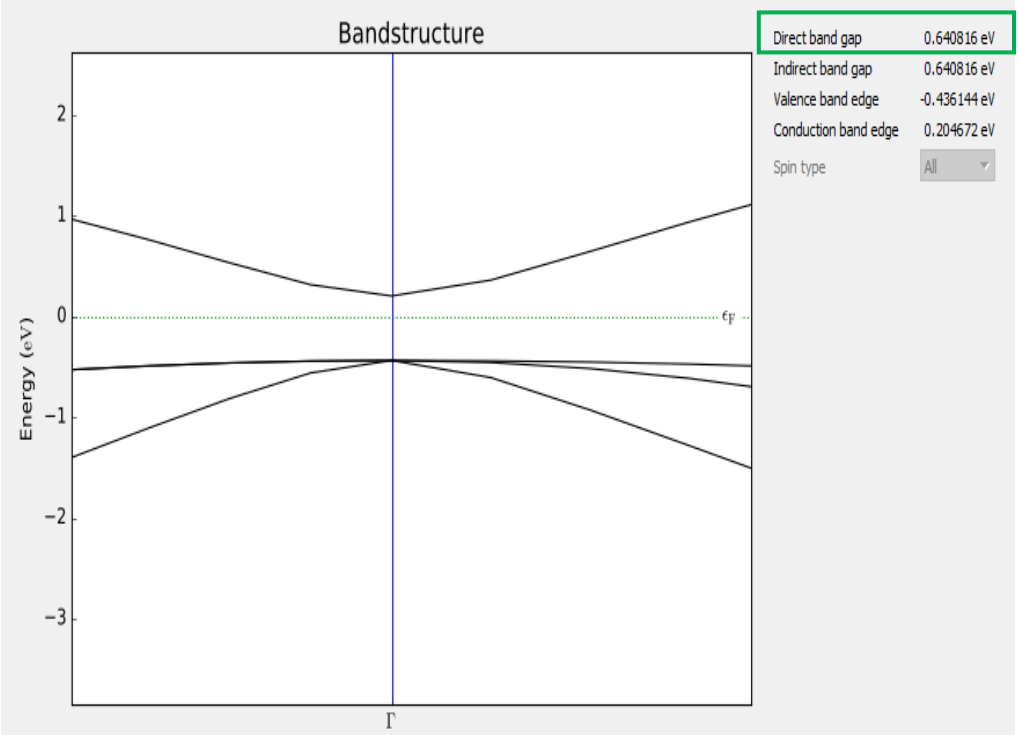

Figure 3.6: Band gap value obtained using LDA.

The band gap value obtained using LDA exchange-correlation functional is 0.64 eV and it is clearly underestimated when compared to the experimental value of 1.5 eV [74]. Since the result obtained is unacceptable, the band structure calculations were performed again using GGA functional. The band gap value obtained using GGA functional was 0.89 eV. Though there was an increase in the band gap value using GGA, where the energy is considered a functional of local density and the gradient of density term is included, this value is still way below compared to the experimental value. The band structure and band gap obtained (using GGA) are shown in figures (3.7) and (3.8) respectively.

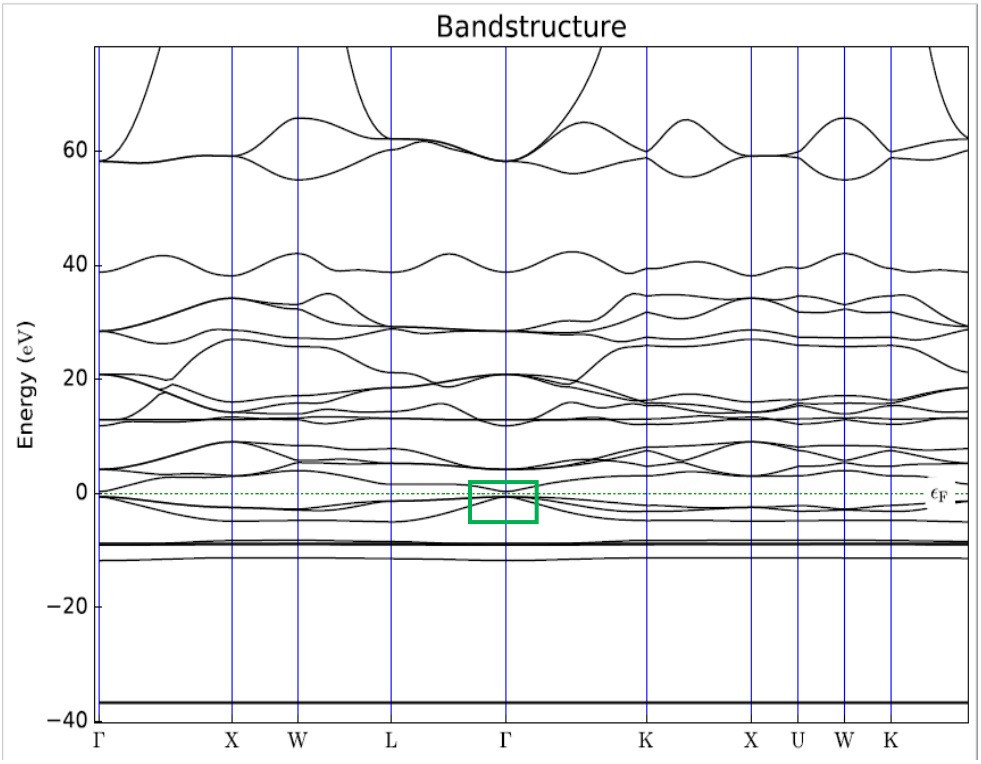

Figure 3.7: Electronic Band structure of CdTe obtained using GGA.

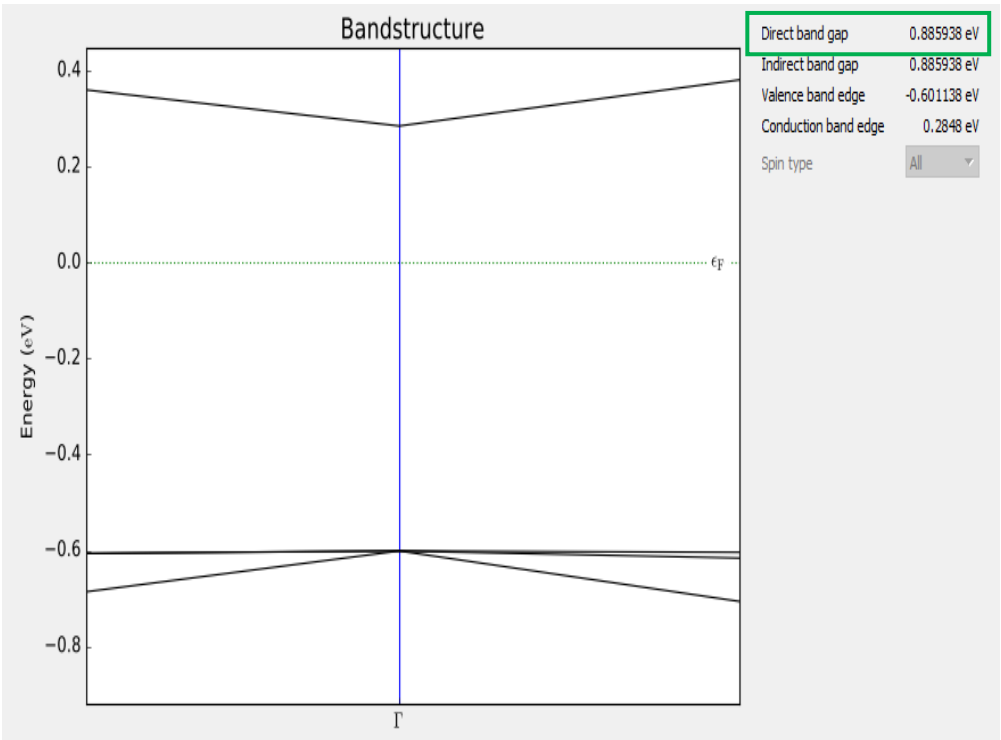

Figure 3.8: Band gap value obtained using GGA.

Table 3.1: Band gap comparison with experimental value for LDA & GGA functionals.

Method Used	Band Gap eV	Percentage Error %
Experiment	1.5± 0.01 **(average value from literature)**	-
LDA	0.64	57.3
GGA	0.89	40.1

3.3.2 Band gaps determined by MGGA and HSE06

So far, the band gap calculated using the standard DFT functionals severely underestimates the value. However, QuantumATK offers more accurate functionals like MGGA, which considers the Laplacian density and Kinetic energy correction term over GGA, and HSE06 hybrid functional that include the mix of Hartree-Fock exchange integral with the GGA exchange-correlation terms.

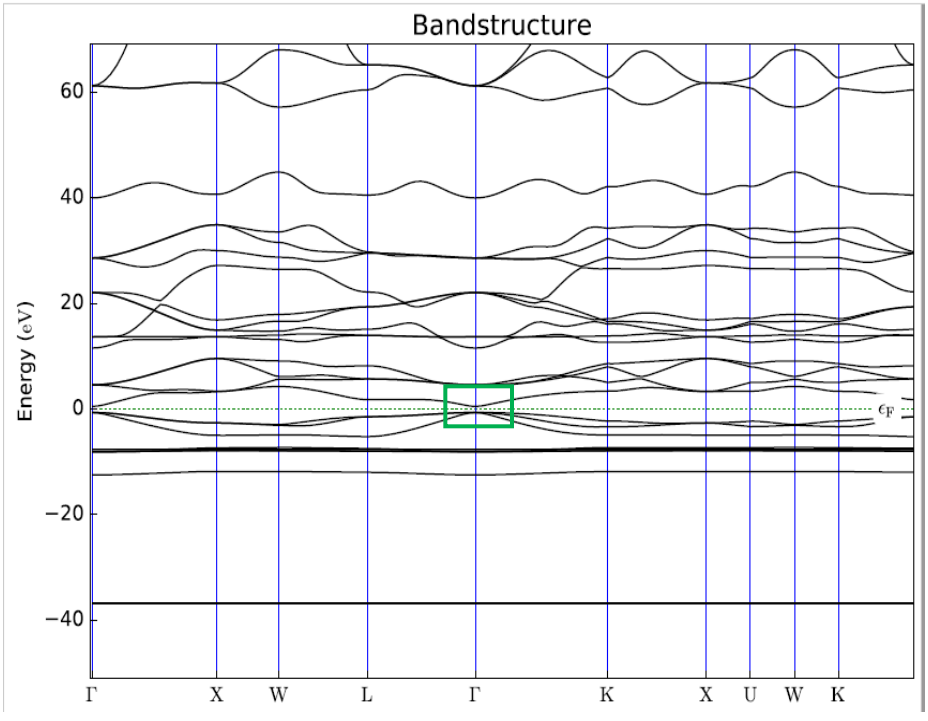

Figure 3.9: Electronic Band structure of CdTe obtained using MGGA.

The MGGA increases the band gap of CdTe over the predicted band gap using GGA. But this value is still underestimated compared to the experimental value and it underestimate it by 24.2%. The band gap value, 1.56 eV obtained using HSE06 hybrid functional increases it significantly by predicting it close to the experimental value of 1.5 eV [74]. HSE06 hybrid functional, expands the KS eigenfunctions using a planewave basis set, which predicts the properties of the bulk systems more accurately. However, the trade of using the hybrid functionals are, higher computation times and costs compared to the LCAO approach.

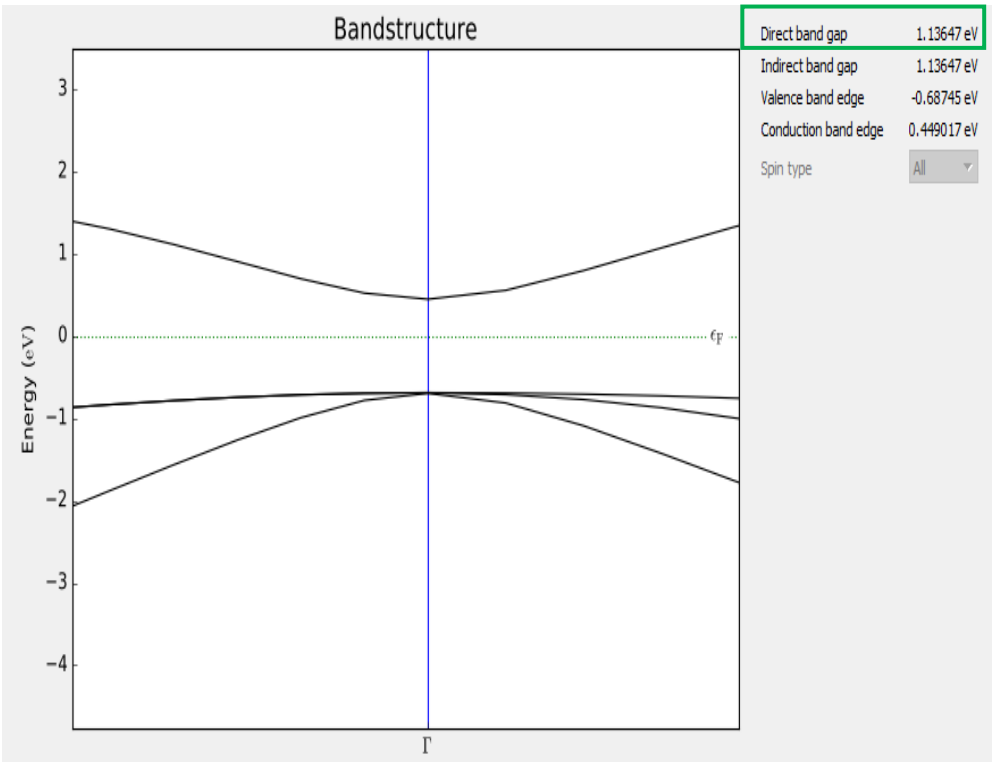

Figure 3.10: Band gap value obtained using MGGA.

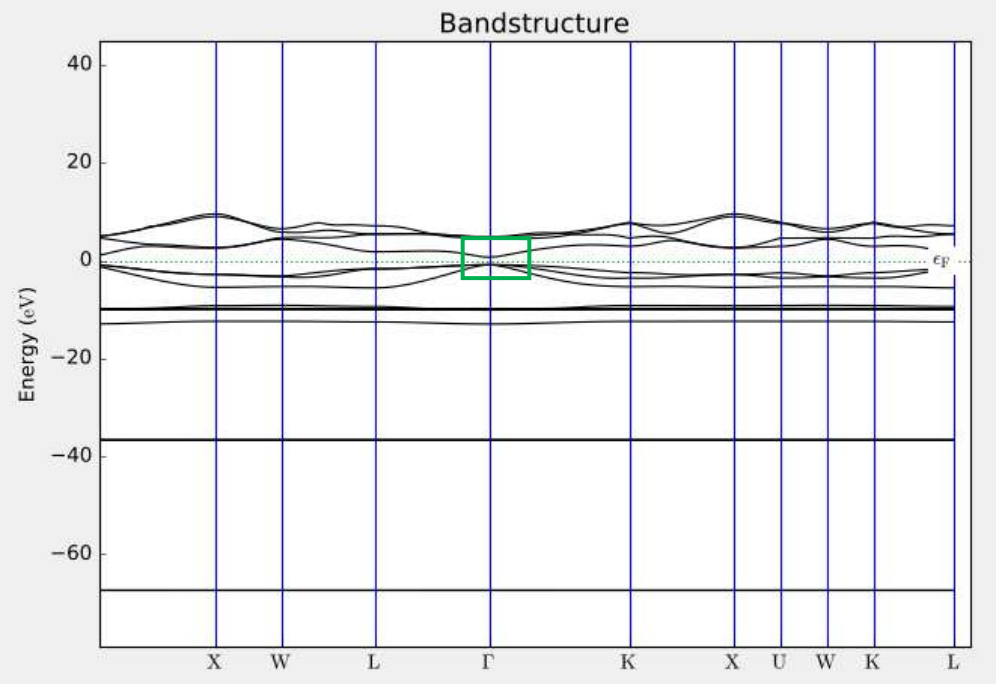

Figure 3.11: Electronic Band structure of CdTe obtained using HSE06.

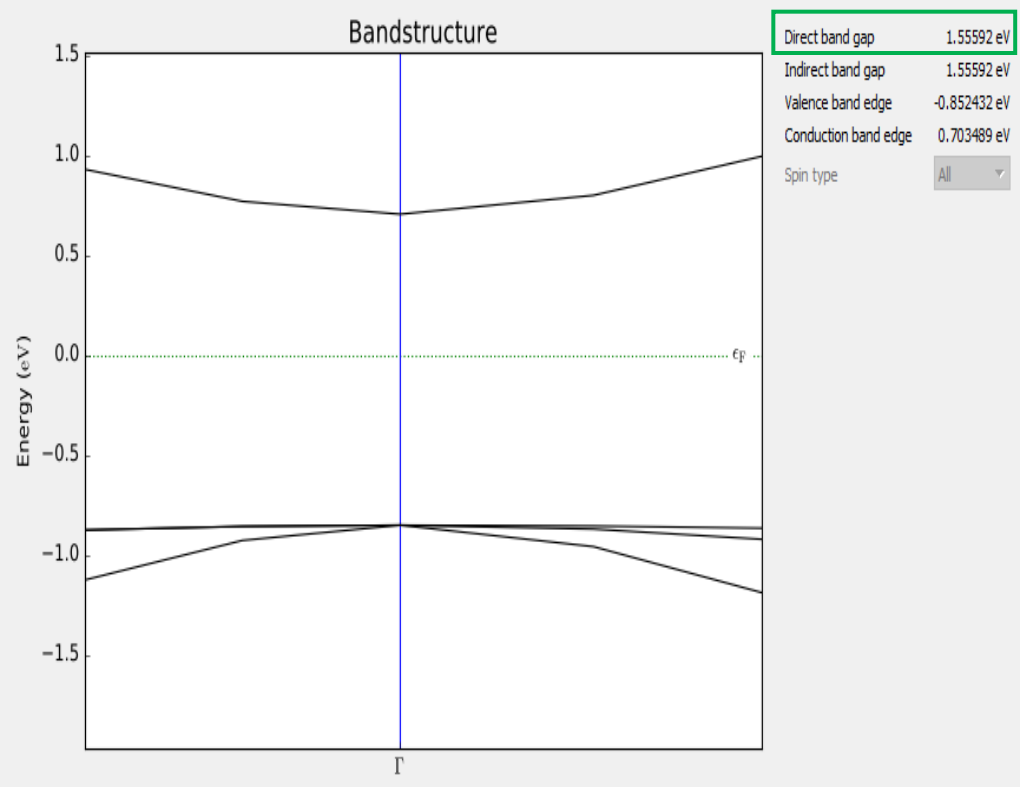

Figure 3.12: Band gap value obtained using HSE06

Table 3.2: Band gap comparison with experimental value for MGGA & HSE06 functionals.

Method Used	**Band Gap eV**	**Percentage Error %**
Experiment	1.5±0.01 **(average value from literature)**	-
MGGA	1.14	24.2 (underpredicts)
HSE06	1.56	3.8 (overpredicts)

3.3.3 Band gaps determined by LDA-1/2 and GGA-1/2

By now we can observe that using more accurate exchange-correlation in QuantumATK, we can approach the experimental band gap of CdTe. Although, the MGGA functional still underestimates the band gap, it is a significant increase over the GGA. HSE06 overpredicts the band gap of CdTe by 3.8% (< 5%) which can be an acceptable value. However, the computational efficiencies are low compared to other functionals used. So, DFT-1/2 method was used to correct the band gaps for the CdTe, with high computational efficiencies. LDA-1/2 and GGA-1/2 functionals solve the band gap problem that is occurred in DFT using Slater half occupation techniques, where a self-energy correction term is used.

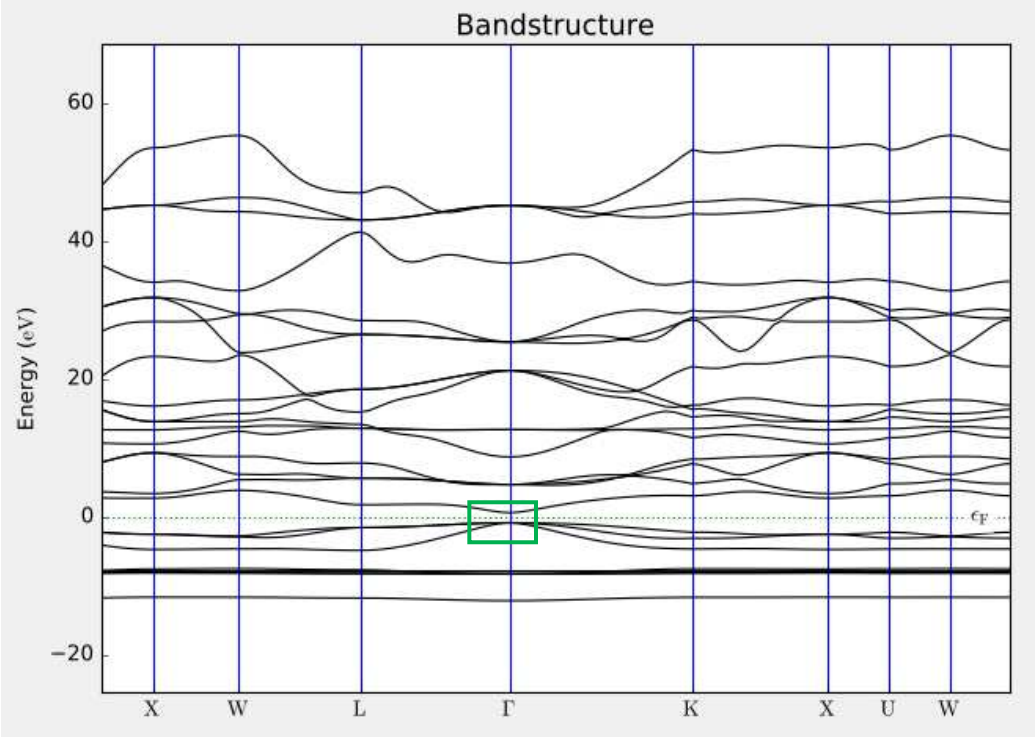

Figure 3.13: Electronic Band structure of CdTe obtained using LDA-1/2.

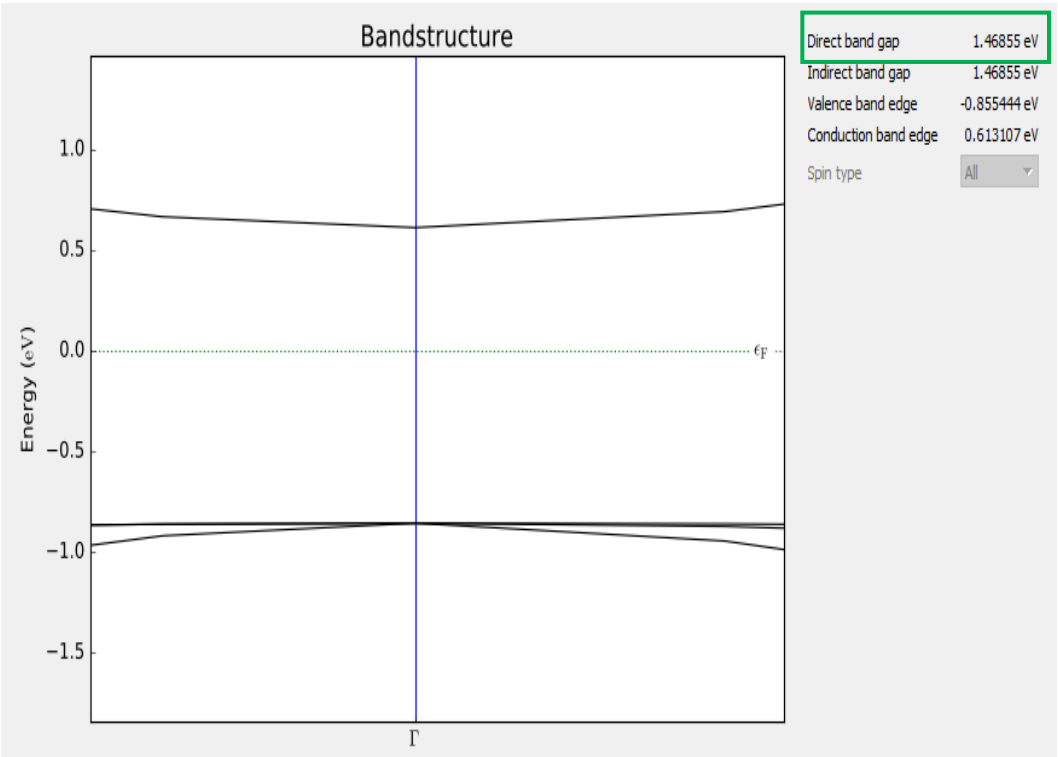

Figure 3.14: Band gap value obtained using LDA-1/2.

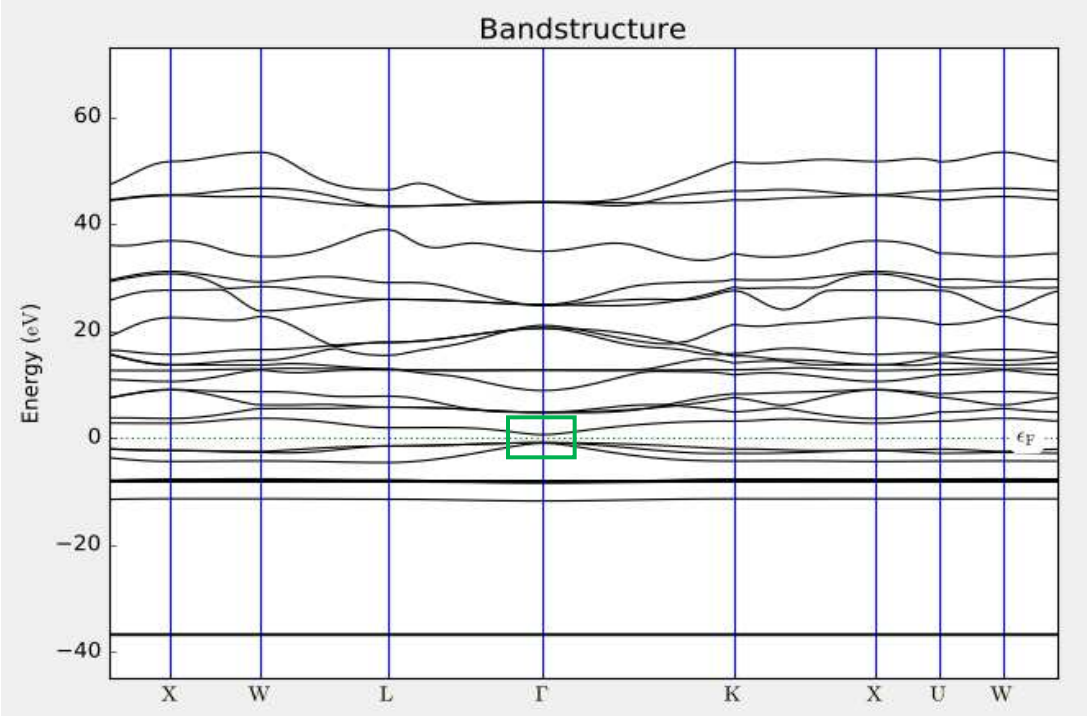

Figure 3.15: Electronic Band structure of CdTe obtained using GGA-1/2.

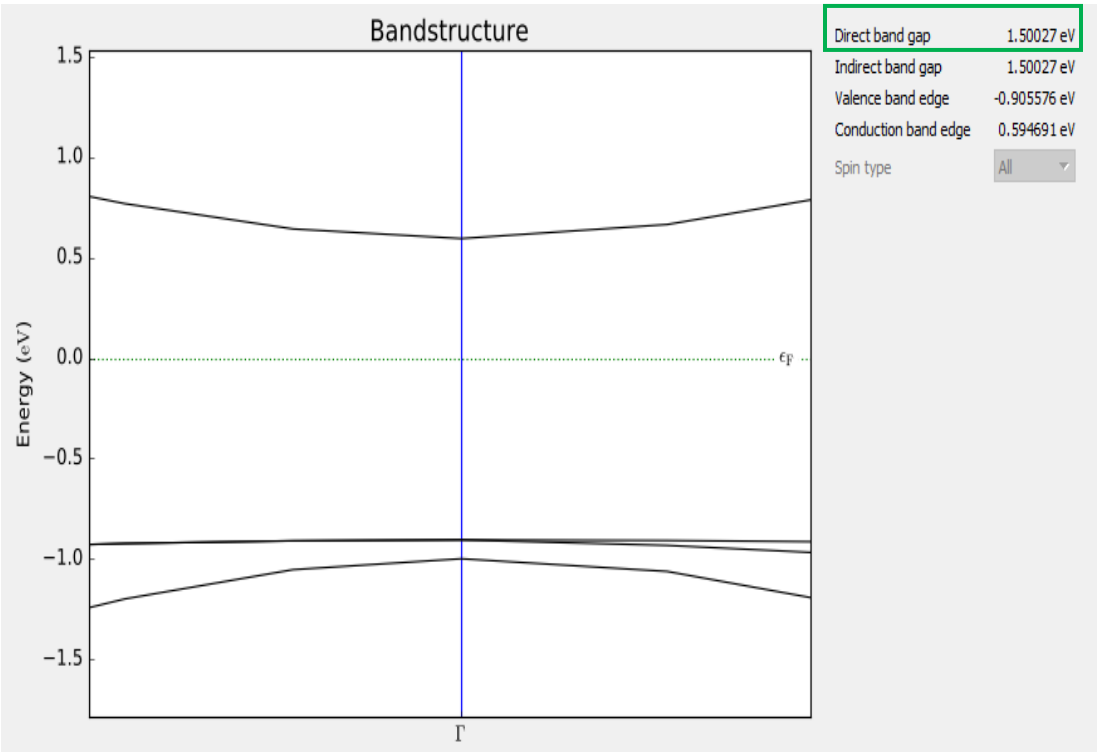

Figure 3.16: Band gap value obtained using GGA-1/2.

Table 3.3: Band gap comparison with experimental value for LDA-1/2 & GGA-1/2 functionals.

Method Used	**Band Gap eV**	**Percentage Error %**
Experiment	1.5 ± 0.01 **(average value from literature)**	-
LDA-1/2	1.47	2
GGA-1/2	1.50	0.02

The band gap value obtained by LDA-1/2 is 1.47 eV, which is 2% less than 1.5 eV [74]. The LDA-1/2 corrects the band gap remarkably. However, GGA-1/2 band gap value is 1.50 eV, which is a serious improvement over the 0.8859 eV predicted by GGA.

3.3.4 Summary of the result

Table 3.4: Summary of band gaps calculated using various exchange-correlation functionals.

Method Used	**Band Gap eV**	**Percentage Error %**
Experiment	1.5 ± 0.01 **(average value from literature)**	-
LDA	0.64	57.3
GGA	0.89	40.1
MGGA	1.14	24.2
HSE06	1.56	3.8
LDA-1/2	1.47	2
GGA-1/2	1.50	0.02

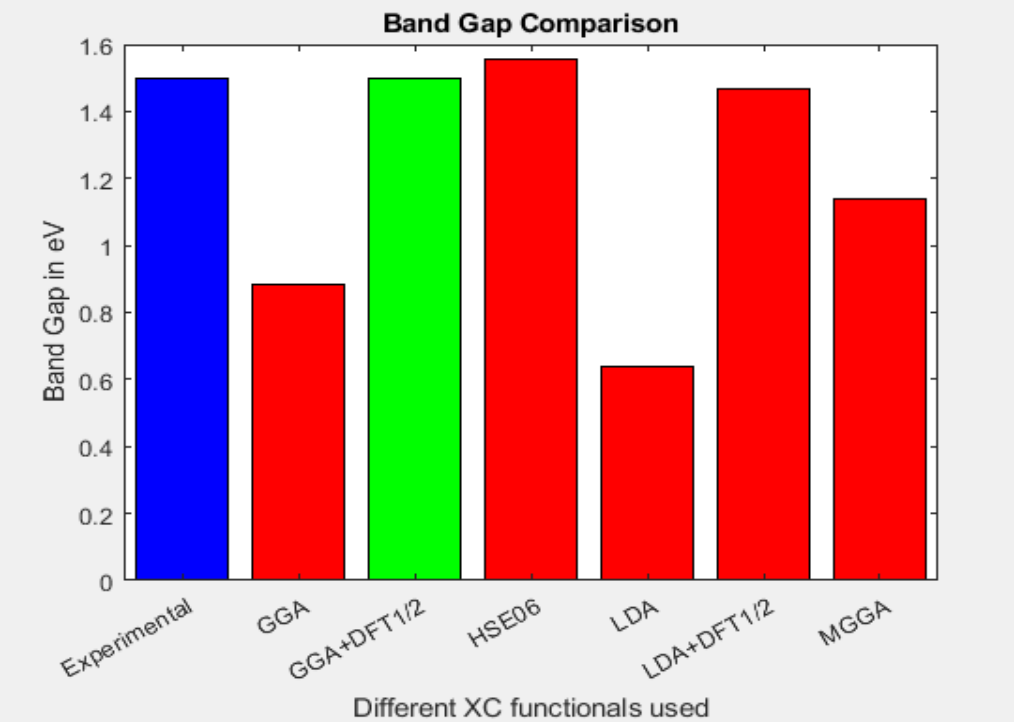

Figure 3.17: Bar graph showing the comparisons of band gaps obtained with various functionals. .

Comparing all the exchange-correlational functionals. The band gaps are improved and are closer to the experimental value of 1.5 eV [74], on using the more accurate exchange-correlation approximation term. Even though the DFT is a theory that describes the band structure for periodic crystals at 0K [6], the band gaps calculated for CdTe using DFT are compared to the experimental band gap value at room temperature in the literature [62][63][64][65][66][67][68][69][70][71][72]. Form the simulations in this study, LDA and GGA underpredicts the band gap. MGGA and HSE06 functionals predicts the band gap with greater accuracy because the approximations for exchange and correlation interactions in these functionals is more accurate. LDA-1/2 corrects the underestimated band gap of CdTe using LDA quite significantly, in QuantumATK, GGA-1/2 predicts the band gap of the CdTe crystal more accurately with just 0.02% error.

CHAPTER 4: CONCLUSIONS AND FUTURE WORK

4.1 Calculations of structural properties of CdTe using QuantumATK

We demonstrated the density functional theory method to calculate the structural properties for CdTe bulk structure. Although using DFT to calculate the structural properties of CdTe is not new, the intention in this work was to use the QuantumATK tool to perform these calculations. To our knowledge, this is done for the first time. Before we perform the calculations to learn the properties of more complicated interfaces of multi-crystalline CdTe thin-film photovoltaics, we first tried to predict the properties of the bulk CdTe crystal using this tool. Firstly, the crystal structure of CdTe in its more stable state, was predicted as desired Zinc-blende structure (FCC) using QuantumATK. This was achieved by comparing the total energies of all possible cubic structures for CdTe. This is the first time to our knowledge, that a work has been done comparing all possible crystal structures of CdTe in order to obtain its most stable structure at equilibrium. QuantumATK has also done a good job in predicting the lattice parameter of the CdTe FCC structure. Different values for lattice constant were obtained using different exchange-correlation functionals, with MGGA being the most accurate. From our knowledge of exchange and correlation approximation available today, the accuracy of the calculated property of a material increases as the accuracy of the approximated term increases. This is clearly was demonstrated with different approximation functionals available in QuantumATK.

4.2 Calculations of the electrical properties of CdTe using QuantumATK

In this preliminary work, we have demonstrated the ability of QuantumATK to predict the band structure of bulk CdTe crystal. DFT when used with standard exchange-correlation approximations, underpredicts the experimental band gap values significantly. Clearly, this was demonstrated with the LDA and GGA approximations used in QuantumATK. The available MGGA and hybrid HSE06 functionals in QuantumATK were used and the band gaps values obtained were higher and closer to the experimental values. However, there was still notable deviations in predicted values from the experimental values. The underestimation of band gaps by DFT, which is most commonly known as band gap problem, was attempted to overcome using the LDA-1/2 and GGA-1/2 approximations. These approximations predicted the band gaps remarkably. GGA-1/2 in particular predicted the band gap of CdTe exceptionally close to the experiment value. Table 4.1 below, summarizes all the calculations performed using QuantumATK in this experiment. The table also compares the results to other data, regarding the properties of CdTe, calculated using different computational tools. All of the data in the references that were used in this comparison was obtained using VASP and Quantum Espresso computational tools.

Table 4.1: Comparison of calculated properties of CdTe in this study to other experimental data available.

Results From	Results Comparisons											
	Different Exchange Correlations Used											
	LDA		GGA		MGGA		LDA-1/2		GGA 1/2		HSE06	
	LP [Å]	BG[eV]	LP [Å]	BG[eV]	LP [Å]	BG[eV]	LP [Å]	BG[eV]	LP [Å]	BG[eV]	LP [Å]	BG[eV]
Applying Quantum ATK to DFT Calculations for CdTe	6.548	0.64	6.614	0.89	6.477	1.14	6.548	1.47	6.614	1.50	–	1.56
Band gap analysis of $CdSe_xTe_{1-x}$, where $0 \leq x \leq 1$ using density functional theory (DFT)methods [62]	–	–	–	–	–	–	–	–	–	–	–	1.55
Electronic Structure & Optical Properties of CdTe [63]	6.529	–	–	–	–	–	–	–	–	–	–	–
Band Structure & Optical Properties of CdTe& CdSn3Te4 [64]	–	–	–	–	–	–	–	–	6.476	1.4	–	–
CdSe/CdTe interface BG & Band Offsets using Spin Orbital [65]	–	0.68	–	–	–	–	–	1.62	–	–	–	–
Electronic Structure of CdTe using GGA+U [66]	–	0.59	–	0.84	–	–	–	–	–	–	–	
LDA/GGA Calculations : Dependence on U parameter [67]	–	0.63	–	0.58	–	–	–	–	–	–	–	1.53
Abinitio calculations of CdSe/CdTe using LDA-1/2 [68]	–	0.68	–	–	–	–	–	1.42	–	–	–	–
Predicting Uncertainty of DFT Approx. properties of CdTe Crystals [69]	6.42	0.61	6.625	0.82	–	–	–	–	–	–	–	1.59
Structural & Electronic Properties of PbTe & CdTe Interfaces [70]	–	–	–	–	–	–	–	1.41	–	–	–	–
Atomistic Simulations of Grain Boundaries in CdTe [71]	–	–	–	0.61	–	–	–	–	–	–	–	–
Special Case of ZnO on CdTe [72]	–	–	6.551	0.68	–	–	–	–	–	–	–	–

LP -: Lattice Parameter in[Å]
BG -: Band Gap in [eV]

From our comparison to the data obtained from other experiments, which used different computational tools, we can conclude that QuantumATK predicts the structural and electrical properties of bulk CdTe very well.

4.3 Future work

In this study we limited the use of QuantumATK to calculate the properties of bulk CdTe. These results obtained, encourages us to extend QuantumATK tool to perform calculations to obtain properties of more complicated interfaces present in multi-crystalline CdTe photovoltaics. However, notable work has already been done on the CdTe/Te and MZO/CdTe interfaces and the future work will involve using QuantumATK for various applications like:

1.) The result will include the Chlorine and Tellurium dioxide passivation layers in one simulation to analyze their effect on band bending and,
2.) Varying the amounts of Magnesium on the MZO/CdTe interface.

REFERENCES

1.) "Publications, P. a. (n.d.). Cadmium Telluride Solar Cells.

2.) Further mention of cost competitiveness: "Solar Power Lightens Up with Thin-Film Technology", Scientific American, April 2008. (n.d.).

3.) Sites, J. (n.d.). Thin Film Solar Cells, by NGPV:Center for Next Generation Photovoltaics . Fort Collins, Colorado , USA.

4.) K. Zweibel, J. Mason, V. Fthenakis, "A Solar Grand Plan", Scientific American, Jan 2008. CdTe PV is the cheapest example of PV technologies and prices are about 16¢/kWh with US Southwest sunlight

5.) *National Renewable Energy Laboratory (NREL), Golden, Co*. (n.d.).

6.) Giustino, F. (2014). *Materials Modelling usinng Density Functional Theory.* Oxford University Press.

7.) Nouredine Zettili (17 February 2009). Quantum Mechanics: Concepts and Applications. John Wiley & Sons. ISBN 978-0-470-02678-6. (n.d.).

8.) "Quantum States of Atoms and Molecules" by David M. Hanson, Erica Harvey, Robert Sweeney, Theresa Julia Zielinski. (n.d.).

9.) Abdulsattar, Mudar A. (2012). "SiGe superlattice nanocrystal infrared and Raman spectra: A density functional theory study". J. Appl. Phys. 111 (4): 044306. Bibcode:2012JAP...111d4306A. doi:10.1063/1.3686610. (n.d.).

10.) Assadi, M. H. N.; et al. (2013). "Theoretical study on copper's energetics and magnetism in TiO2 polymorphs". Journal of Applied Physics. 113 (23): 233913–233913–5. arXiv:1304.1854. Bibcode:2013JAP...113w3913A. doi:10.1063/1.4811539. (n.d.). *Journal of Applied Physics*.

11.) Boudec, J. Y. L.; McDonald, D.; Mundinger, J. (2007). "A Generic Mean Field Convergence Result for Systems of Interacting Objects". Fourth International Conference on the Quantitative Evaluation of Systems (QEST 2007) (PDF). p. 3. doi:10.1109/QEST.2007.8. (n.d.).

12.) Antony, J., Grimme, S.: Phys. Chem. Chem. Phys. 8, 5287–5293 (2006). (n.d.).

13.) Baccelli, F.; Karpelevich, F. I.; Kelbert, M. Y.; Puhalskii, A. A.; Rybko, A. N.; Suhov, Y. M. (1992). "A mean-field limit for a class of queueing networks". Journal of Statistical Physics. 66 (3–4): 803. Bibcode:1992JSP....66..803B. doi:10.1007/BF0105570. (n.d.).

14.) Becke, Axel D. (1988). "Density-functional exchange-energy approximation with correct asymptotic behavior". Physical Review A. 38 (6): 3098–3100. (n.d.).

15.) Griffiths, David J. (2004), Introduction to Quantum Mechanics (2nd ed.), Prentice Hall, ISBN 978-0-13-111892-8. (n.d.).

16.) Born, M., & Huang, K. (1955). Dynamical theory of crystal lattices. Oxford: Oxford University Press. (n.d.).

17.) Born, M., & Oppenheimer, J. R. (1927). Zur Quantentheorie der molekeln. Annalen der Physik, 84, 457. (n.d.).

18.) Collins, M. A., & Parsons, D. F. (1993). Implications of rotation-inversion-permutation invariance for analytic molecular potential energy surfaces. The Journal of Chemical Physics, 99, 6756. (n.d.).

19.) Brooks, R.E., Bruccoleri, B.R., Olafson, B.D., States, D.J., Swaminathan, S., Karplus, M.: J. Comput. Chem. 4, 187–217 (1983). (n.d.).

20.) Chaikin, P. M.; Lubensky, T. C. (2007). Principles of condensed matter physics (4th print ed.). Cambridge: Cambridge University Press. ISBN 978-0-521-79450-3. (n.d.).

21.) Dreuw, A., Weisman, J.L., Head-Gordon, M.: J. Chem. Phys. 119, 2943–2946 (2003). (n.d.).

22.) Ferreira, L. G. (2008). Approximation to density functional theory for the calculation of band gaps of semiconductors.

23.) https://docs.quantumatk.com/manual/ATKDFT.html#sect2-atkdft-dfthalf.

24.) Combes, J. M., & Seiler, R. (1980). Spectral properties of atomic and molecular systems. In R. G. Woolley (Ed.), Quantum dynamics of molecules. NATO ASI B57 (p. 435). New York: Plenum. (n.d.). *Quantum dynamics of molecules*.

25.) Gasiorowicz, S. (2019). Quantum Physics. 2nd ed. Canada: Hamilton Printing, pp.1-50. (n.d.).

26.) Gell-Mann, M., Bruecker, K.A.: Phys. Rev. 106, 364–368 (1957). (n.d.).

27.) Kresse, G., & Joubert, D. (1999). From ultrasoft pseudopotentials to the projector augmented-wave method". Physical Review B. 59 (3): 1758–1775.

28.) Grimme, M., Steinmetz, S., Korth, M.: J. Org. Chem. 72, 2118–2126 (2007). (n.d.).

29.) J.M.Soler,E.Artacho,J.D. Gale,A.Garcia, J.Junquera,P.Ordejon,and F.Sanchez-Portal, J.Phys.Conden.Matter 14 2745. (2002).

30.) Grimme, Stefan (2004). "Accurate description of van der Waals complexes by density functional theory including empirical corrections". Journal of Computational Chemistry. 25 (12): 1463–1473. doi:10.1002/jcc.20078. PMID 15224390. (2004). *Journal of Computational Chemistry*.

31.) Hamann, D. R.; Schlüter, M.; Chiang, C. "Norm-Conserving Pseudopotentials". Physical Review Letters. 43 (20): 1494–1497. (1997).

32.) Hartree, D. R.; Hartree, W. (1935). "Self-consistent field, with exchange, for beryllium". Proc. Royal Soc. Lond. A. 150 (869): 9. doi:10.1098/rspa.1935.0085. (n.d.).

33.) *https://docs.quantumatk.com/tutorials*. (n.d.). Retrieved from QuantumATK .

34.) J. B. Foresman and *Æ*. Frisch, Exploring Chemistry with Electronic Structure Methods, Gaussian, Pittsburgh, 1995-96, p 102. (n.d.).

35.) A. Milani, E. Bocchi, A. Zappettini, S.M. Pietralunga, M. Martinelli, J. Cryst. Growth 214/215, 913(2000).

36.)Khutoryansky, E. (2016, April 15). *PATREON*. Retrieved from https://www.patreon.com/EugeneK

37.) Krieger, J.B., Chen, J., Iafrate, G.J., Savin, A.: In: Gonis, A., Kioussis, N., Ciftan, M. (eds.) Electron Correlations and Materials Properties. Plenum, New York (1999). (n.d.).

38.) J.F. Janak, Phys. Rev. B 18, 7165 (1978).

39.) Luiz G. Ferreira, M. M. (2011). Slater half-occupation technique revisited: the LDA-1/2 and GGA-1/2 approaches for atomic ionization energies and band gaps in semiconductors.

40.) M. L. Cohen, J. R. (1988). "Electronic Structure and Optical Spectra of Semiconductors.

41.) Mean-Field Theory: Hartree-Fock and BCS in E. Pavarini, E. Koch, J. van den Brink, and G. Sawatzky: Quantum materials: Experiments and Theory, Jülich 2016, ISBN 978-3-95806-159-0. (n.d.).

42.) Omar, M. Ali (1994). Elementary Solid State Physics, 4th ed. Addison Wesley. ISBN 978-0-201-60733-8. (n.d.).

43.) Pearlman, D.A., Case, D.A., Caldwell, J.W., Ross, W.S., Cheatham, T.E. III, DeBolt, S., Ferguson, D., Seibel, G., Kollman, P.: Comput. Phys. Commun. 91, 1–41 (1995). (n.d.).

44.) Van Mourik, Tanja; Gdanitz, Robert J. (2002). "A critical note on density functional theory studies on rare-gas dimers". Journal of Chemical Physics. 116 (22): 9620–9623. Bibcode:2002JChPh.116.9620V. doi:10.1063/1.1476010. (2002). *Journal of Chemical Physics*. Perdew, J.P., Ruzsinszky, A., Tao, J., Staroverov, V.N., Scuseria, G.E., Csonka, G.I.: J. Chem. Phys. 123, 062201(1–9) (2006). (n.d.).

45.) Schrödinger, E. (1926). "Quantisierung als Eigenwertproblem; von Erwin Schrödinger". Annalen der Physik. 384 (4): 361–377. Bibcode:1926AnP...384..361S. doi:10.1002/andp.19263840404. (n.d.).

46.) Perdew, John P.; Chevary, J. A.; Vosko, S. H.; Jackson, Koblar A.; Pederson, Mark R.; Singh, D. J.; Fiolhais, Carlos (1992). "Atoms, molecules, solids, and surfaces: Applications of the generalized gradient approximation for exchange and correlation". Phy. (n.d.). *Applications of the generalized gradient approximation for exchange and correlation*.

47.) Pickett, Warren E. (April 1989), "Pseudopotential methods in condensed matter applications", Computer Physics Reports. (n.d.).

48.) Press, O. B. (1995). The interpretation of quantum mechanics: Dublin seminars (1949–1955).

49.) Sakurai, J. J. (1995). Modern Quantum Mechanics. Reading, Massachusetts: Addison-Wesley. p. 68. (n.d.).

50.) Schrodinger equation". Hyperphysics. Department of Physics and Astronomy, George State University. (n.d.).

51.) Schrödinger, E. (1926). Retrieved 25th August 2013. *An Undulatory Theory of Mechanics of Atoms and Molecules*.

52.)Schwerdtfeger, P. (August 2011), "The Pseudopotential Approximation in Electronic Structure Theory", ChemPhysChem, 12 (17): 3143–3155. (n.d.).

53.) V. Dobrosavljevic. Introduction to Metal-Insulator Transitions. Conductor Insulator Quantum Phase Transitions. Oxford University Press, 2012. (n.d.).

54.) Ward, D. and Volkmer, S. (2019). How to Derive the Schrodinger Equation. [online] arXiv.org. Available at: https://arxiv.org/abs/physics/0610121v1 [Accessed 29 May 2019] . (n.d.).

55.) Shankar, R. (1943). Principles of Quantum Mechanics (2nd ed.). Kluwer Academic/Plenum Publishers. ISBN 978-0-306-44790-7. (n.d.).

56.) Sherrill, C. D. (2000). *An Introduction to Hartree-Fock Molecular Orbital Theory by C. David Sherrill (June 2000).*

57.)Slater, J. C. (1930). "Note on Hartree's Method". Phys. Rev. 35 (2): 210. doi:10.1103/PhysRev.35.210.2. (n.d.).

58.)*Up and Atom*. (2018, July 6). Retrieved from https://www.youtube.com/watch?v=QeUMFo8sODk

59.) Wigner, E.P., Seitz, F.: Phys. Rev. 43, 804–810 (1933). (n.d.).

60.) QuantumATK: An integrated platform of electronic and atomic-scale modellin tools. (2019).

61.) A. H. Munshi, N. Sasidharan, S. Pinkayan, K. L. Barth, W. Sampath, and W. Ongsakul, “Thin-film CdTephotovoltaics –The technology for utility scale sustainable energy generation,” Sol. Energy, vol. 173, pp. 511 –516, 2018. Band gap analysis of $CdSe_xTe_{1-x}$, where $0 \leq x \leq 1$ using density functional theory (DFT)methods, Evie Ingold, Thomas Fiducia, John M.Walls, Michael j. Watts, Pooja Goddard, and Roger Smith.

62.) Band gap analysis of CdST, where 0 1 using density functional theory (DFT)methods.

63.) Structural and Optical Properties of CdTe Thin Films Deposited Using RF Magnetron Sputtering, Rupali Kulkarni, Sachin Rondiya, Amit Pawbake, Ravindra Waykar, Ashok Jadhavar, Vijaya Jadkar, Ajinkya Bhorde, Abhijit Date, Habib Pathan, Sandesh Jadkar.

64.) Band structure and Optical properties CdTe and CdSn3Te4 thin films, Thangamuthu Venkatachalem.

65.) CdSe/CdTe interface band gaps and band offsets calculated using spin–orbit and self-energy corrections M.Ribeiro Jr., L.G. Ferreira, L.R.C. Fonseca, R. Ramprasad.

66.) Electronic structure of CdTe using GGA+U E. Menéndez-Proupin, A. Amézaga, N.Cruz Hernández.

67.) LDA+*U*/GGA+*U* calculations of structural and electronic properties of CdTe: Dependence on the effective *U* parameter Yelong Wu, Guangde Chen, Youzhang Zhu, Wan-Jian Yin, Yanfa Yan, Mowafak Al-Jassim, Stephen J. Pennycook.

68.) Ab initio calculation of the CdSe/CdTe heterojunction band offset using the local-density approximation-1/2 technique with spin-orbit corrections, M.Ribeiro Jr., L.G. Ferreira, L.R.C. Fonseca, R. Ramprasad.

69.) Predicting Uncertainty of Density Functional Approximations for Properties of Crystals with Cubic Symmetry.

70.) Structural & Electronic Properties of PbTe & CdTe Interfaces, R.Leitsmann, F. Bechstedt, H. Groiss, F. Schaffler, W. Heiss, K. Koike, H. Harada, M. Yano.

71.) Atomistic Simulations of Grain Boundaries in CdTe, Faith G.Sen, Christopher Buurma, Tadas Paulauskas, Ce Sun, Moon Kim, Sivalingma Sivananthan, Robert F.Klie, Maria K.Y. Chan.

72.) Band offsets for mismatched interfaces: The special Case of ZnO on CdTe, John E. Jaffe, Tiffany C.Kaspar, and Timothy C. Droubay.

73.) A.E. Merad, M.B. Kanoun , G. Merad, J Cibert, H. Aourag Full-potential investigation of the electronic properties and optical properties of stressed CdTe and ZnTe Mater. Chem. Phys, 92 (2005), pp.333-339

74.) D.E. Swanson, J.R. Sites and W.S. Sampath, Solar Energy Materials and Solar cells 159 (2017)